nature communications

Article

https://doi.org/10.1038/s41467-025-68009-4

The interconnected wirings between medial prefrontal cortex and claustrum and their governing roles in the methamphetamine reward memory in male mice

Received: 15 May 2025

Accepted: 15 December 2025

Published online: 12 January 2026

Check for updates

Yuhong He[1,4], Ziheng Zhao[1,4], Yang Liu[1,4], Quying Feng[1], Sijia Wang[1,2], Wenzhong Wu[2], Hee Young Kim[3], Yu Fan[1] ✉ & Xiaowei Guan[1] ✉

Bidirectional communication between medial prefrontal cortex (mPFC) and claustrum (CL) plays a critical role in drug reward memory, particularly for conditioned drug-associated cues. However, their precise circuitry remains unclear. Here, using viral tracing, chemo-&opto-genetics and patch-clamp, alongside methamphetamine (METH) conditioned place preference (CPP) model, we dissected the connectivity pattern between mPFC and CL in male mice. Two relatively independent pathways of top-down mPFC-CL and bottom-up CL-mPFC were identified, each comprising both direct excitatory and indirect inhibitory projections. The mPFC-CL pathway predominantly mediates inter-hemispheric communication, while the CL-mPFC pathway mainly supports intra-hemispheric connections. Under physiological conditions, strong feedforward inhibition (FFI) via local GABAergic interneurons suppresses excitatory transmission between mPFC and CL. During METH CPP, FFI is weakened, resulting in enhanced excitatory signaling. The mPFC-CL pathway was engaged during reward memory encoding, whereas the CL-mPFC pathway mediated memory retrieval. These findings suggest potential therapeutic interventions for METH reward memory.

The brain operates as a highly interconnected wirings, which supports various cognitive and behavioral functions. Although high-tech brain science and technology have accelerated the understanding of brain networks, there are still questions that need to be clarified about structural connections, functional interactions, and efficiency connections in brain networks. As a highly addictive psychostimulant, methamphetamine (METH) abuse remains a global crisis[1]. The addictive potential of METH arises from its ability to profoundly influence the reward circuits in the brain, leading to euphoric and reinforcing effects[2,3]. Chronic METH use is tightly linked to specific environmental settings, forming strong contextual associations with METH rewards[4,5]. The conditioned place preference (CPP) is a widely used behavioral paradigm to assess drug reward learning and environmental cue associations[6]. The CPP procedure contains two main phases: the training phase establishes (encodes) the association of the environment cue with the drug's rewarding effects, while the test phase measures the retrieval of drug-context reward memory[7].

Recently, the interconnectivity of medial prefrontal cortex (mPFC) with the claustrum (CL) has gained much attention in substance use disorders, due to its crucial role in reward-based learning and memory[8,9]. The mPFC is a high-level executive region of the brain, being essential for decision-making, cognitive flexibility, impulsive control,

[1]Department of Human Anatomy and Histoembryology, Nanjing University of Chinese Medicine, Nanjing, China. [2]Jiangsu Province Hospital of Chinese Medicine, Affiliated Hospital of Nanjing University of Chinese Medicine, Nanjing, China. [3]Department of Physiology, Yonsei University College of Medicine, Seoul, South Korea. [4]These authors contributed equally: Yuhong He, Ziheng Zhao, Yang Liu. ✉e-mail: yfan@njucm.edu.cn; guanxw918@njucm.edu.cn

reward encoding and motivation[10]. The mPFC is composed primarily of glutamatergic (Glu) neurons ($mPFC^{Glu}$) and a small proportion of gamma-aminobutyric acid (GABA) interneurons ($mPFC^{GABA}$)[11]. These $mPFC^{GABA}$ neurons are crucial for maintaining the excitatory/inhibitory (E/I) balance of $mPFC^{Glu}$ neurons[12,13]. Hu et al. proposed that maintaining the E/I balance in the mPFC during the process of memory retrieval might represent an effective therapeutic strategy for the treatment of METH addiction[14]. The CL is a thin sheet-like subcortical brain structure buried between insula and putamen, densely connecting the cortical regions with other subcortical regions, serving as a hub for its role in multisensory integration, attention and consciousness[15–17]. Similar to the mPFC, the CL consists of approximately 90% CL^{Glu} neurons and about 10% CL^{GABA} neurons[18]. Recent emerging evidence, including ours, demonstrates that the CL plays an important role in drug-craving and seeking behaviors as well as withdrawal symptoms, which might be driven by its role in integrating environmental cue information in the drug reward process[9,19,20]. There exist abundant projection connections between mPFC and CL, with Glu neurons being dominant[21], forming the top-down mPFC-CL pathway and the bottom-up CL-mPFC pathway. Recently, several research groups have begun to identify the interconnection patterns between mPFC and CL, as well as their role in the reward process and neurological disorders. For example, the CL provides strong and long-lasting feedforward inhibition (FFI) of the prefrontal cortex (PFC), and plays a unique role in regulating cognitive processes in prefrontal circuits[22]. In addition, optogenetic activation of the CL-prelimbic cortex (PL) pathway suppresses the chronic social defeat stress-induced depressive-like behaviors in male mice[23]. These studies suggest that the reciprocal projections between mPFC and CL involves in the process of drug reward memory, particularly for conditioned drug-associated cues. However, their precise neural circuits and the principles established therein remain unclear, leading to poorly understanding of their roles in reward.

In the current study, using viral tracing, fiber photometry, chemo-&opto-genetics and patch-clamp, alongside METH CPP model, we dissected the connectivity pattern between mPFC and CL from the view of whole brain, including the direct and indirect pathways, interhemispheric and intra-hemispheric communication, the overlapped receiving and projecting Glu neurons in each local region, and the physiological intermodulation between the two regions. Further, we explored the distinct governing roles of the top-down mPFC-CL and the bottom-up CL-mPFC pathways in the encoding and retrieval processes of the METH reward-associated environment context.

Results

Reciprocal projections between mPFC and CL

To validate the reciprocal connections between mPFC and CL from a whole-brain perspective, we performed a fluorescent micro-optical sectioning tomography (fMOST) experiment. As shown in Fig. 1a, b and Supplementary Fig. 1a, b, mPFC fibers chiefly projected to the contralateral CL, while CL fibers primarily targeted the ipsilateral mPFC.

For the top-down mPFC-CL pathway, as shown in Supplementary Fig. 1c, d, anterograde labeling from mPFC showed EGFP-positive axon terminals were predominantly localized in contralateral CL. As shown in Supplementary Fig. 1e, f, retrograde labeling from CL revealed mCherry-positive somas were mainly in contralateral mPFC. For the bottom-up CL-mPFC pathway, as shown in Supplementary Fig. 1g, h, anterograde labeling from CL showed EGFP-positive axon terminals were predominantly in the ipsilateral mPFC. As shown in Supplementary Fig. 1i, j, retrograde labeling from mPFC revealed mCherry-positive somas were mainly observed in ipsilateral CL.

Independent features in interconnectivity between mPFC and CL

First, we identified the neuronal populations that send efferents and receive afferents within the mPFC-CL circuits (Fig. 1c–j). As shown in Fig. 1c, d and Supplementary Fig. 1k, l, projection-specific viral tracing revealed two distinct populations of mPFC neurons, as indicated by mCherry-positive neurons projecting to CL (top-down pathway) and EGFP-positive neurons receiving inputs from CL (bottom-up pathway). Minimal overlap between these two populations, which indicates that the projecting neurons and the receiving neurons within the mPFC are distinct populations. As shown in Fig. 1e, f, it was about 73.5% of $mPFC^{Glu}$ neurons while 17.4% $mPFC^{GABA}$ neurons that received afferents from CL, implying CL-$mPFC^{Glu}$ pathway and CL-$mPFC^{GABA}$ pathway. By contrast, about 92.3% of neurons that send efferents to CL were $mPFC^{Glu}$ neurons. A similar investigation was carried out to identify CL neurons (Fig. 1g, h and Supplementary Fig. 1m, n), as indicated by mCherry-positive neurons projecting to mPFC and EGFP-positive neurons receiving inputs from mPFC. Minimal overlap between these two populations, which indicates that the projecting neurons and the receiving neurons within the CL are distinct populations. As shown in Fig. 1i, it was about 67.3% of CL^{Glu} neurons while 24.9% CL^{GABA} neurons that received afferents from mPFC, implying mPFC-CL^{Glu} pathway and mPFC-CL^{GABA} pathway. By contrast, about 91.8% of neurons that send efferents to mPFC were CL^{Glu} neurons (Fig. 1j). Together, these results indicate that projecting neurons and input-receiving neurons are largely distinct within both mPFC and CL. These projecting neurons are mainly Glu, while the receiving population consisted of a mixture of Glu and GABA neurons.

Second, we used electrophysiological patch-clamp recording to investigate the potential microcircuit architecture and functional connectivity between the mPFC and CL (Figs. 2 and 3). As shown in Fig. 2a and Supplementary Fig. 2a, b, the EGFP-labeled CL^{GABA} neurons, while dense mCherry-labeled $mPFC^{Glu}$ terminals within CL. As shown in Fig. 2b, c, both excitatory postsynaptic currents (oEPSCs) and inhibitory postsynaptic currents (oIPSCs) were induced on CL^{Glu} neurons when opto-stimulating $mPFC^{Glu}$ terminals. Both oEPSCs and oIPSCs of CL^{Glu} neurons were abolished by incubating tetrodotoxin (TTX) in the ACSF, and the oEPSCs but not oIPSCs were reintroduced by the application of 4-aminopyridine (4-AP). As shown in Fig. 2d, e, bath application of picrotoxin (PTX) blocked the oIPSCs but not oEPSCs, while bath application of 2,3-Dihydroxy-6-nitro-7-sulfamoyl-benzo (f) quinoxaline (NBQX) and D-2-Amino-5-phosphonovaleric acid (AP5) blocked both oEPSCs and oIPSCs of CL^{Glu} neurons. These results suggest that $mPFC^{Glu}$ neurons make monosynaptic excitatory connections and disynaptic inhibitory connections with CL^{Glu} neurons. When opto-stimulating $mPFC^{Glu}$ terminals, the oEPSCs were induced on CL^{GABA} neurons, which were abolished by TTX and then reintroduced by 4-AP and abolished again by bath application of NBQX and AP5 (Fig. 2f–h). These results suggest that $mPFC^{Glu}$ neurons make monosynaptic excitatory connections with CL^{GABA} neurons. Then, we verified the monosynaptic connections from CL^{GABA} neurons to CL^{Glu} neurons. As shown in Fig. 2i and Supplementary Fig. 2c, d, the EYFP-labeled CL^{GABA} neurons that received $mPFC^{Glu}$ terminals. When opto-stimulating CL^{GABA} neurons, the oIPSCs were induced on CL^{Glu} neurons, which were abolished by TTX, reintroduced by 4-AP and then abolished by PTX again (Fig. 2j, k). These results suggest that CL^{GABA} neurons make monosynaptic inhibitory connections with CL^{Glu} neurons. Taken together, these patch-clamp results verified the existence of $mPFC^{Glu}$-CL^{Glu} direct excitatory pathway and $mPFC^{Glu}$-CL^{GABA}-CL^{Glu} indirect inhibitory pathway.

Similarly, as shown in Fig. 3a and Supplementary Fig. 2e, f, the EGFP-labeled $mPFC^{GABA}$ neurons, while dense mCherry-labeled CL^{Glu} terminals within mPFC. As shown in Fig. 3b, c, both oEPSCs and oIPSCs were induced on $mPFC^{Glu}$ neurons when opto-stimulating CL^{Glu} terminals. Both oEPSCs and oIPSCs of $mPFC^{Glu}$ neurons were abolished by incubating TTX in the ACSF, and the oEPSCs but not oIPSCs were reintroduced by the application of 4-AP. As shown in Fig. 3d, e, bath application of PTX blocked the oIPSCs but not oEPSCs, while bath application of NBQX and AP5 blocked both oEPSCs and oIPSCs of

https://doi.org/10.1038/s41467-025-68009-4

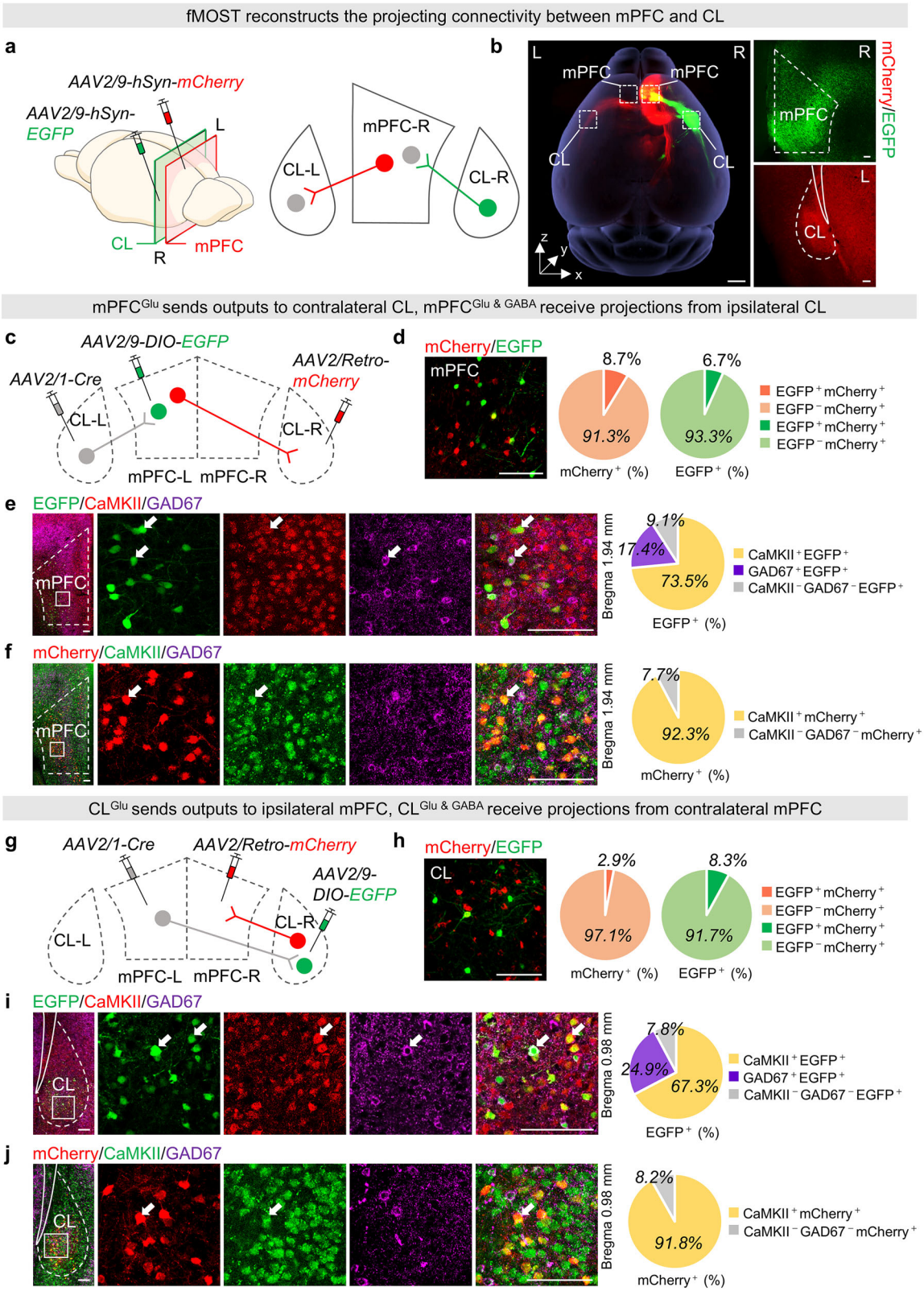

Fig. 1 | mPFC and CL project onto each other. a Schematic diagram of virus injection and experimental flow chart. **b** Representative image of viral transfection site in mPFC and CL ($n = 1$). **c** Schematic diagram of virus injection and viral expression. **d** Co-labeling statistics of EGFP- and mCherry-positive neurons in mPFC ($n = 3$). **e** Co-labeling statistics of EGFP-positive neurons with CaMKII- and GAD67-positive neurons in mPFC ($n = 3$). **f** Co-labeling statistics of mCherry-positive neurons with CaMKII- and GAD67-positive neurons in mPFC ($n = 3$). **g** Same as (**c**). **h** Same as (**d**) but in CL ($n = 3$). **i** Same as (**e**) but in CL ($n = 3$). **j** Same as (**f**) but in CL ($n = 3$). Scale bar, 1 mm (**b**) or 100 μm (**b**, **d**–**f**, **h**–**j**). Source data are provided as a Source Data File.

https://doi.org/10.1038/s41467-025-68009-4

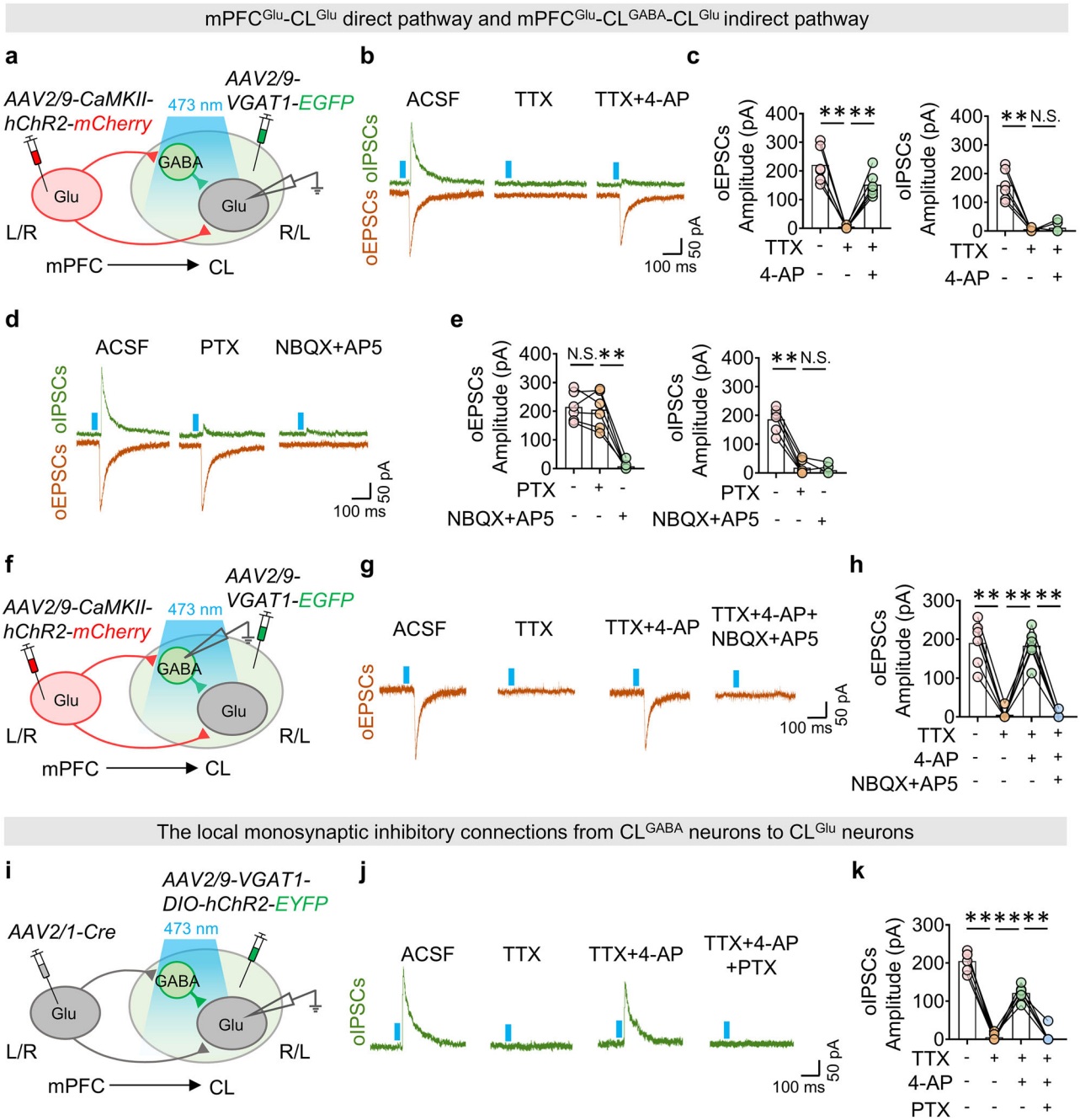

Fig. 2 | The mPFC-CL pathway has strong feedforward inhibitory effects. **a** Schematic diagram of the CL^{Glu} neurons under patch clamp recording. **b** Representative traces of the amplitude showing the oEPSCs and oIPSCs in CL^{Glu} neurons. **c** Representative quantification of the amplitude showing the oEPSCs and oIPSCs in CL^{Glu} neurons. The amplitude of oEPSCs, two-tailed paired *t*-test, $n = 6$ cells from 4 mice, TTX, $t_{(5)} = 8.2530$, $p = 0.0004$ vs. ACSF; TTX + 4-AP, $t_{(5)} = 8.6950$, $p = 0.0003$ vs. TTX. The amplitude of oIPSCs, two-tailed paired *t*-test, $n = 6$ cells from 4 mice, TTX, $t_{(5)} = 6.7940$, $p = 0.0011$ vs. ACSF; TTX + 4-AP, $t_{(5)} = 1.1320$, $p = 0.3089$ vs. TTX. **d** Same as (**b**). **e** Same as (**c**). The amplitude of oEPSCs, two-tailed paired *t*-test, $n = 6$ cells from 4 mice, PTX, $t_{(5)} = 0.5786$, $p = 0.5879$ vs. ACSF; NBQX + AP5, $t_{(5)} = 7.8830$, $p = 0.0005$ vs. PTX. The amplitude of oIPSCs, two-tailed paired *t*-test, $n = 6$ cells from 4 mice, PTX, $t_{(5)} = 12.9800$, $p < 0.0001$ vs. ACSF; NBQX + AP5, $t_{(5)} = 0.9956$, $p = 0.3652$ vs. PTX. **f** Same as (**a**) but in CL^{GABA} neurons. **g** Same as (**b**) but of oEPSCs in CL^{GABA} neurons. **h** Same as (**c**) but of oEPSCs in CL^{GABA} neurons. Two-tailed paired *t*-test, $n = 6$ cells from 4 mice, TTX, $t_{(5)} = 8.7600$, $p = 0.0003$ vs. ACSF; TTX + 4-AP, $t_{(5)} = 10.2700$, $p = 0.0002$ vs. TTX; TTX + 4-AP + NBQX + AP5, $t_{(5)} = 11.9500$, $p < 0.0001$ vs. TTX + 4-AP. **i** Same as (**a**). **j** Same as (**b**) but of oIPSCs in CL^{Glu} neurons. **k** Same as (**c**) but of oIPSCs in CL^{Glu} neurons. Two-tailed paired *t*-test, $n = 6$ cells from 4 mice TTX, $t_{(5)} = 21.4500$, $p < 0.0001$ vs. ACSF; TTX + 4-AP, $t_{(5)} = 11.7100$, $p < 0.0001$ vs. TTX; TTX + 4-AP + PTX, $t_{(5)} = 9.5430$, $p = 0.0002$ vs. TTX + 4-AP. All statistical tests are two-sided. Data presented as mean ± SEM. N.S., $p > 0.05$, $^{*}p < 0.05$, $^{**}p < 0.01$. Source data are provided as a Source Data File.

$mPFC^{Glu}$ neurons. These results suggest that CL^{Glu} neurons make monosynaptic excitatory connections and disynaptic inhibitory connections with $mPFC^{Glu}$ neurons. When opto-stimulating CL^{Glu} terminals, the oEPSCs were induced on $mPFC^{GABA}$ neurons, which were abolished by TTX and then reintroduced by 4-AP and abolished again by bath application of NBQX and AP5 (Fig. 3f–h). These results suggest that CL^{Glu} neurons make monosynaptic excitatory connections with $mPFC^{GABA}$ neurons. Then, we verified the monosynaptic connections from $mPFC^{GABA}$ neurons to $mPFC^{Glu}$ neurons. As shown in Fig. 3i and Supplementary Fig. 2g, h, the EYFP-labeled $mPFC^{GABA}$ neurons that

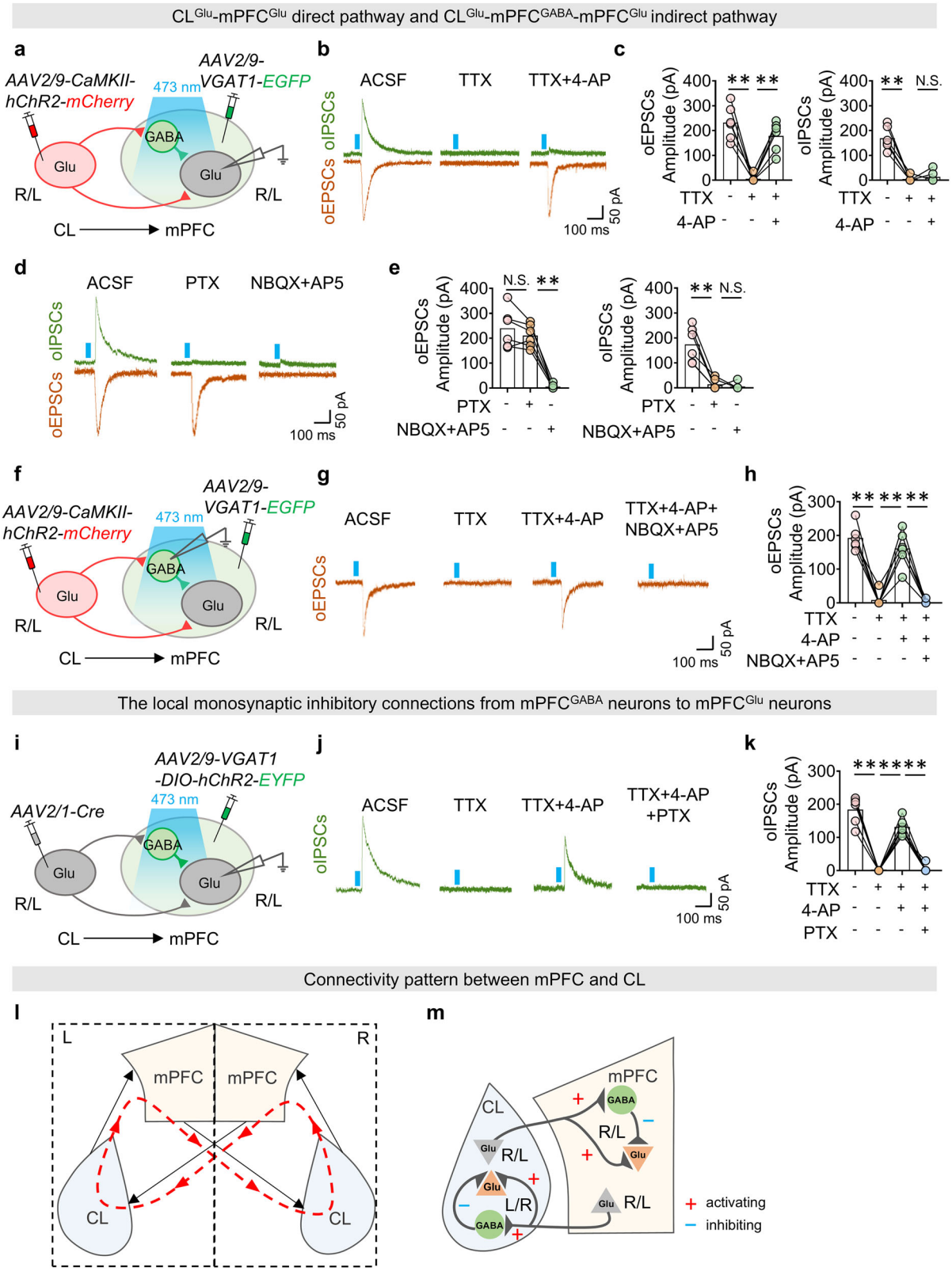

received CL^{Glu} terminals. When opto-stimulating mPFC^{GABA} neurons, the oIPSCs were induced on mPFC^{Glu} neurons, which were abolished by TTX, reintroduced by 4-AP and then abolished by PTX again (Fig. 3j, k). These results suggest that mPFC^{GABA} make monosynaptic inhibitory connections with mPFC^{Glu} neurons. Taken together, these patch-clamp results verified the existence of CL^{Glu}-mPFC^{Glu} direct excitatory pathway and CL^{Glu}-mPFC^{GABA}-mPFC^{Glu} indirect inhibitory pathway.

Collectively, there are four independent pathways between mPFC and CL across the two cerebral hemispheres, the top-down mPFC-CL pathway which primarily facilitates communication between the left and right hemispheres of the brain, as well as the bottom-up CL-mPFC pathway that predominantly connects regions within the ipsilateral hemisphere (Fig. 3l). As shown in Fig. 3 m, in either top-down pathway of mPFC-CL or bottom-up pathway of CL-mPFC, there exist both direct

Fig. 3 | The CL-mPFC pathway exerts strong feedforward inhibitory effects. **a** Schematic diagram of the $mPFC^{Glu}$ neurons under patch clamp recording. **b** Representative traces of the amplitude showing the oEPSCs and oIPSCs in $mPFC^{Glu}$ neurons. **c** Representative quantification of the amplitude showing the oEPSCs and oIPSCs in $mPFC^{Glu}$ neurons. The amplitude of oEPSCs, two-tailed paired *t*-test, $n = 6$ cells from 3 mice, TTX, $t_{(5)} = 7.3000$, $p = 0.0008$ vs. ACSF; TTX + 4-AP, $t_{(5)} = 7.3840$, $p = 0.0007$ vs. TTX. The amplitude of oIPSCs, two-tailed paired *t*-test, $n = 6$ cells from 3 mice, TTX, $t_{(5)} = 8.1740$, $p = 0.0004$ vs. ACSF; TTX + 4-AP, $t_{(5)} = 0.7363$, $p = 0.4946$ vs. TTX. **d** Same as (**b**). **e** Same as (**c**). The amplitude of oEPSCs, two-tailed paired *t*-test, $n = 6$ cells from 4 mice, PTX, $t_{(5)} = 1.7700$, $p = 0.1370$ vs. ACSF; NBQX + AP5, $t_{(5)} = 11.2400$, $p < 0.0001$ vs. PTX. The amplitude of oIPSCs, two-tailed paired *t*-test, $n = 6$ cells from 4 mice, PTX, $t_{(5)} = 5.5510$, $p = 0.0026$ vs. ACSF; NBQX + AP5, $t_{(5)} = 0.6732$, $p = 0.5307$ vs. PTX. **f** Same as (**a**) but in $mPFC^{GABA}$ neurons. **g** Same as (**b**) but of oEPSCs in $mPFC^{GABA}$ neurons. **h** Same as (**c**) but of oEPSCs in $mPFC^{GABA}$ neurons. Two-tailed paired *t*-test, $n = 6$ cells from 4 mice, TTX, $t_{(5)} = 9.6090$, $p = 0.0002$ vs. ACSF; TTX + 4-AP, $t_{(5)} = 6.7430$, $p = 0.0011$ vs. TTX; TTX + 4-AP + NBQX + AP5, $t_{(5)} = 7.4510$, $p = 0.0007$ vs. TTX + 4-AP. **i** Same as (**a**). **j** Same as (**b**) but of oIPSCs in $mPFC^{Glu}$ neurons. **k** Same as (**c**) but of oIPSCs in $mPFC^{Glu}$ neurons. Two-tailed paired *t*-test, $n = 6$ cells from 4 mice, TTX, $t_{(5)} = 11.0100$, $p = 0.0001$ vs. ACSF; TTX + 4-AP, $t_{(5)} = 12.8300$, $p < 0.0001$ vs. TTX; TTX + 4-AP + PTX, $t_{(5)} = 9.3460$, $p = 0.0002$ vs. TTX + 4-AP. **l** There are four independent pathways between mPFC and CL of the two cerebral hemispheres, which are connected anterogradely to form an unclosed circuit. **m** In either top-down mPFC-CL pathway or bottom-up CL-mPFC pathway, there exist direct excitatory pathways and indirect inhibitory pathways between $mPFC^{Glu}$ neurons and CL^{Glu} neurons. All statistical tests are two-sided. Data presented as mean ± SEM. N.S., $p > 0.05$, $^{**}p < 0.01$. Source data are provided as a Source Data File.

excitatory pathways and indirect inhibitory pathways between $mPFC^{Glu}$ neurons and CL^{Glu} neurons, forming Glu-Glu pathways and Glu-GABA-Glu pathways in mPFC-CL circuits. The projecting Glu neurons are rarely overlapped with the receiving Glu neurons in each region of connectivity pathways between mPFC and CL, which are connected anterogradely to form an unclosed circuit.

Physiological regulation of the mPFC-CL circuits

To investigate functional connectivity between mPFC and CL in vivo, we monitored neuronal activity during pathway-specific activation (Fig. 4 and Supplementary Fig. 3). For the top-down mPFC-CL pathway (Fig. 4a, b and Supplementary Fig. 3a), activation of mPFC neurons significantly increased the activity of CL^{GABA} neurons, while suppressing CL^{Glu} neurons (Fig. 4c, d and Supplementary Fig. 3b, c). Similarly, for the bottom-up CL-mPFC pathway (Fig. 4e, f and Supplementary Fig. 3d), when activating the CL neurons enhanced $mPFC^{GABA}$ neuronal activity and reduced $mPFC^{Glu}$ neuronal activity (Fig. 4g, h and Supplementary Fig. 3e, f).

These results indicate that both top-down (mPFC-CL) and bottom-up (CL-mPFC) pathways exhibited a reciprocal pattern under physiological conditions, Glu neurons at one end negatively regulated Glu neuronal activity at the other end. This effect is likely mediated by strong FFI via GABAergic interneurons in the mPFC-CL circuits (Fig. 4i, j).

Activity phenotypes of $mPFC^{Glu}$ and CL^{Glu} in METH CPP

To investigate the neural activity in mPFC and CL under pathological conditions, we established a METH CPP model in male mice. After 8 days of CPP-Training, the mice exhibited a significantly increased preference for the drug-paired chambers (Fig. 5a, b and Supplementary Fig. 4a, b). Following CPP-Test, the ramp-shaped action potentials (APs) were recorded in slices containing mPFC and CL. Compared with that of saline group, the number of APs in mPFC and CL neurons of METH group was significantly higher after ramp-shaped injection of cellular current (Fig. 5c–f and Supplementary Fig. 4c, d). In addition, as shown in Supplementary Fig. 4e–h, compared with saline group, both the c-Fos (a marker of neuronal activation)-positive $mPFC^{Glu}$ neurons and c-Fos-positive CL^{Glu} neurons were significantly increased, while the c-Fos-positive $mPFC^{GABA}$ neurons and c-Fos-positive CL^{GABA} neurons remained unchanged after CPP-Test in METH group mice.

Next, the oEPSCs and oIPSCs of $mPFC^{Glu}$ neurons and CL^{Glu} neurons along the interconnectivity circuits between mPFC and CL were recorded in saline group and METH group after CPP-Test (Fig. 5j–l). As shown in Fig. 5g–i, compared with that in saline group, the oEPSCs amplitude was significantly increased, while the oIPSCs amplitude of CL^{Glu} neurons was significantly decreased in METH group mice. As shown in Fig. 5j–l, compared with that in saline group, the oEPSCs amplitude was significantly increased, while the oIPSCs amplitude of $mPFC^{Glu}$ neurons was significantly decreased in METH group mice.

These results indicate that the neuronal activities of $mPFC^{Glu}$ neurons, $mPFC^{GABA}$ neurons, CL^{Glu} neurons and CL^{GABA} neurons during METH CPP-Test have changed compared with the physiological state. As for the indirect pathways along mPFC-CL and CL-mPFC interconnectivity, it seems that the inhibitory effects of both CL^{GABA} micro-projections on CL^{Glu} neurons and $mPFC^{GABA}$ micro-projections on $mPFC^{Glu}$ neurons were weakened following CPP-Test in METH group mice, which leads to a synchronous increase in the activities of $mPFC^{Glu}$ neurons and CL^{Glu} neurons (Fig. 5m, n).

The top-down mPFC-CL pathway contributes to the encoding of METH reward memory during the process of METH CPP-Training

To investigate the role of the mPFC-CL pathway in METH CPP, the top-down pathway was regulated during METH CPP-Training period (Group 1 and Group 3) or during METH CPP-Test period (Group 2 and Group 4).

First, we performed chemogenetic manipulation to suppress the mPFC neurons along the mPFC-CL pathway (Fig. 6a, b and Supplementary Fig. 5a, b). As shown in Supplementary Fig. 5c, d, approximately 50% transfection rate in $mPFC^{Glu}$ neurons and clozapine-N-oxide (CNO) can effectively reduce mPFC neuronal activity. As shown in Supplementary Fig. 5e, f, compared to the Veh-treated mice of METH group (M-Veh group), the CNO-treated mice of METH group (M-CNO group) during CPP-Training period (Group 1) effectively reduced the percentage of c-Fos-positive CL^{Glu} neurons, but this effect was not observed during CPP-Test period (Group 2). However, the M-CNO group during either CPP-Training period (Group 1) or CPP-Test period (Group 2) had no effect on the percentage of c-Fos-positive CL^{GABA} neurons (Supplementary Fig. 5g, h). As shown in Fig. 6c, d (Group 1), compared to the corresponding Veh group, inhibiting the mPFC neurons projecting to CL during CPP-Training period had no effect on CPP score and ΔCPP score in the CNO-treated mice of saline group (S-CNO group), but effectively reduced the CPP score and ΔCPP score in M-CNO group. There was no difference in the total distance traveled among the four groups of mice. However, as shown in Fig. 6e, f (Group 2), when inhibiting these neurons during CPP-Test period, compared to the corresponding Veh group, both S-CNO group and M-CNO group exhibited similar CPP score and ΔCPP score. There was no significant difference in the total distance traveled among the four groups of mice. Additionally, chemogenetic inhibition of $mPFC^{Glu}$ terminals in the CL during CPP-Training period also reduced the CPP score and ΔCPP score in M-CNO group mice (Supplementary Fig. 6a–d), and effectively suppressed the activity of Glu neurons in the CL (Supplementary Fig. 6e, f) following CNO infusion.

Then, we found that the CL^{GABA} neurons in the mPFC-CL pathway showed significantly reduced activity during CPP-Training period in METH group mice when compared to the saline group mice, while the CL^{GABA} neurons activity had no significant changes during CPP-Test period (Supplementary Fig. 7a–c). Specifically, activating the CL^{GABA}

https://doi.org/10.1038/s41467-025-68009-4

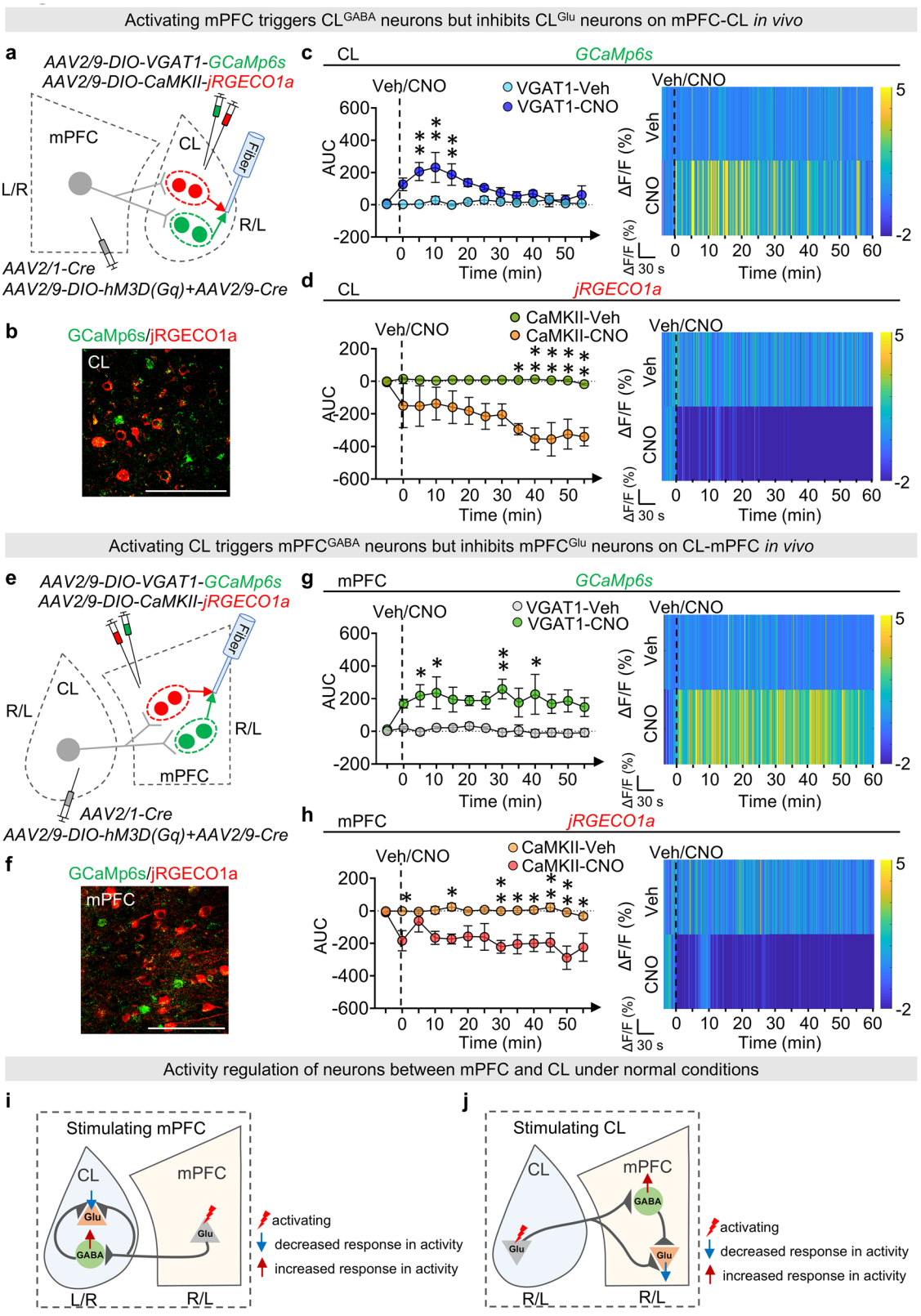

neurons along the mPFC-CL pathway through chemogenetic regulatory techniques (Fig. 6g, h and Supplementary Fig. 8a, b). As shown in Supplementary Fig. 8c, d, with 60% transfection rate in CL^{GABA} neurons and CNO can effectively enhance CL neuronal activity. As shown in Supplementary Fig. 8e, f, compared to the M-Veh group, the M-CNO group during CPP-Training period (Group 3) effectively reduced the percentage of c-Fos-positive CL^{Glu} neurons, but this effect was not observed during CPP-Test period (Group 4). As shown in Fig. 6i, j (Group 3), compared to the corresponding Veh group, activating the CL^{GABA} neurons that receive projections from mPFC during CPP-Training period effectively reduced the CPP score and ΔCPP score in M-CNO group, and had no effect on CPP score and ΔCPP score in S-CNO group. There was no difference in the total distance traveled among the four groups of mice. However, as shown in Fig. 6k, l

Fig. 4 | Under physiological conditions, the mPFC-CL circuits exhibit opposing changes in upstream and downstream Glu activities, but parallel changes between upstream Glu and downstream GABA activities. a Schematic diagram of virus injection and viral expression in mPFC-CL pathway. **b** Representative image of virus injection in CL. **c** The quantification of AUC (two-way ANOVA, $n = 4$, $F_{(12, 78)} = 2.4190$, $p = 0.0101$) and heatmap of GCaMp6s fluorescence in CL. **d** The quantification of AUC (two-way ANOVA, $n = 4$, $F_{(12, 78)} = 1.4440$, $p = 0.1646$) and heatmap of jRGECO1a fluorescence in CL. **e** Same as (**a**) but in CL-mPFC pathway. **f** Same as (**b**) but in mPFC. **g** The quantification of AUC (two-way ANOVA, $n = 4$, $F_{(12, 78)} = 0.7318$, $p = 0.7163$) and heatmap of GCaMp6s fluorescence in mPFC. **h** The quantification of AUC (two-way ANOVA, $n = 4$, $F_{(12, 78)} = 1.3330$, $p = 0.2173$) and heatmap of jRGECO1a fluorescence in mPFC. Under physiological conditions, in both top-down (**i**) and bottom-up (**j**) pathways between mPFC and CL, the Glu neurons at one end have a negative regulatory effect on the Glu neurons at the other, which might be due to the strong FFI effects of GABA neuronal activity through the indirect inhibitory pathways. Scale bar, 100 μm (**b**, **f**). All statistical tests are two-sided. Data presented as mean ± SEM. $^{*}p < 0.05$, $^{**}p < 0.01$. Source data are provided as a Source Data File.

(Group 4), when activating these neurons during CPP-Test period compared to the corresponding Veh group, both S-CNO group and M-CNO group exhibited similar CPP score and ΔCPP score. There was no significant difference in the total distance traveled among the four groups of mice.

These results suggest that the top-down mPFC-CL pathway is involved in the encoding association of METH with drug-paired CPP context which was established during METH CPP-Training period, rather than the process of METH reward memory retrieval during METH CPP-Test period.

The bottom-up CL-mPFC pathway contributes to the retrieval of METH reward memory during the process of METH CPP-Test

To explore the role of the CL-mPFC pathway in METH CPP, the bottom-up pathway was regulated during METH CPP-Training period (Group 5 and Group 7) or during METH CPP-Test period (Group 6 and Group 8).

First, inhibiting the CL neurons along the CL-mPFC pathway through chemogenetic regulatory techniques (Fig. 7a, b and Supplementary Fig. 9a, b). As shown in Supplementary Fig. 9c, d, approximately 50% transfection rate in CL^{Glu} neurons and CNO can effectively reduce CL neuronal activity. As shown in Supplementary Fig. 9e, f, compared to the M-Veh group, the M-CNO group during CPP-Test period (Group 6) could effectively reduce the percentage of c-Fos-positive $mPFC^{Glu}$ neurons, but this effect was not observed during CPP-Training period (Group 5). However, the M-CNO group during either CPP-Training period (Group 5) or CPP-Test period (Group 6) had no effect on the percentage of c-Fos-positive $mPFC^{GABA}$ neurons (Supplementary Fig. 9g, h). As shown in Fig. 7c, d (Group 5), when inhibiting the CL neurons projecting to mPFC during CPP-Training period, both S-CNO group and M-CNO group exhibited similar CPP score and ΔCPP score when compared to the corresponding vehicle group. There was no significant difference in the total distance traveled among the four groups of mice. However, as shown in Fig. 7e, f (Group 6), compared to the corresponding Veh group, inhibiting these neurons during CPP-Test period effectively reduced the CPP score and ΔCPP score in M-CNO group, and had no effect on CPP score and ΔCPP score in S-CNO group. There was no difference in the total distance traveled among the four groups of mice. As depicted in Supplementary Fig. 10a–c, when compared to corresponding Pre-Test score, CNO infusion during CPP-Test 1 (on Day 9) significantly reduced CPP score in METH-CNO group mice, and effectively inhibited the activity of Glu neurons within the mPFC (Supplementary Fig. 10d–g) following CNO infusion, indicating that the suppression of CL^{Glu} terminals in the CL-mPFC pathway could block the retrieval of METH reward memory. While, during CPP-Test 2 (on Day 10) that performed after CNO clearance, CPP score was once again elevated relative to CPP-Test 1 levels in METH-CNO group mice, indicating a reactivation of the previously acquired CPP memory (Supplementary Fig. 10c).

Then, we found that the $mPFC^{GABA}$ neurons in the CL-mPFC pathway showed significantly reduced activity during CPP-Test period in METH group mice when compared to the saline group mice, while the $mPFC^{GABA}$ neurons had no significant changes during CPP-Training period (Supplementary Fig. 11a–c). Specifically, we performed chemogenetic manipulation to activate the $mPFC^{GABA}$ neurons along the CL-mPFC pathway (Fig. 7g, h and Supplementary Fig. 12a, b). As shown in Supplementary Fig. 12c, d, approximately 60% transfection rate in $mPFC^{GABA}$ neurons and CNO can effectively enhance mPFC neuronal activity. As shown in Supplementary Fig. 12e, f, compared to the M-Veh group, the M-CNO group during CPP-Test period (Group 8) could effectively reduce the percentage of c-Fos-positive $mPFC^{Glu}$ neurons, but this effect was not observed during CPP-Training period (Group 7). As shown in Fig. 7i, j (Group 7), compared to the corresponding vehicle group, when activating the $mPFC^{GABA}$ neurons that receive projections from CL during CPP-Training period, both S-CNO group and M-CNO group exhibited similar CPP score and ΔCPP score. However, as shown in Fig. 7k, l (Group 8), compared to the corresponding vehicle group, activating these neurons during CPP-Test period effectively reduced the CPP score and ΔCPP score in M-CNO group, and had no effect on CPP score and ΔCPP score in S-CNO group. There was no significant difference in the total distance traveled among the four groups of mice.

These results suggest that the bottom-up CL-mPFC pathway is involved in the retrieval of METH reward memory which was established during METH CPP-Test period, rather than the association process of METH with drug-paired CPP context during METH CPP-Training period.

Discussion

In the current study, the interconnected wirings between mPFC and CL and their governing role in METH reward memory were explored in male mice. We found that there existed two relatively independent pathways: the top-down mPFC-CL pathway which primarily facilitates communication between the left and right hemispheres of the brain, as well as the bottom-up CL-mPFC pathway that predominantly connects regions within the ipsilateral hemisphere. In mPFC-CL circuits, there contains direct excitatory pathway and indirect inhibitory pathway, forming Glu-Glu pathways and Glu-GABA-Glu pathways. It is worth noting that the projecting Glu neurons and the receiving Glu neurons in each region along the pathways are rarely overlapped, forming an unclosed circuit between mPFC and CL. Under physiological conditions, the local $mPFC^{GABA}$ or CL^{GABA} interneurons exert a robust FFI on the $mPFC^{Glu}$ or CL^{Glu} neurons along the indirect inhibitory pathways between mPFC and CL, resulting a negative regulatory effect over Glu neurons between mPFC and CL. Under the METH CPP model, both $mPFC^{Glu}$ and CL^{Glu} neurons were triggered in male mice, at least in part due to the weakened FFI of GABAergic interneurons on the indirect inhibitory pathways between mPFC and CL. The top-down mPFC-CL pathway involves the encoding process of METH with the METH-related context which was established during CPP-Training, while the bottom-up CL-mPFC pathway contributes to the retrieval of METH-related context memory which is carried out when CPP-Test (Fig. 8).

In this study, we observed hemispheric asymmetry in the connectivity pattern between mPFC and CL, as indicated that mPFC mainly send projections to the contralateral CL, whereas CL projections predominantly send projections to the ipsilateral mPFC. Although the cerebral hemispheres are structurally similar, they exhibit functional lateralization in cognitive processes, including memory. Some studies have demonstrated that different types of memory information are predominantly encoded by distinct hemispheres. For instance, the left PFC is more strongly implicated in episodic memory encoding, while

https://doi.org/10.1038/s41467-025-68009-4

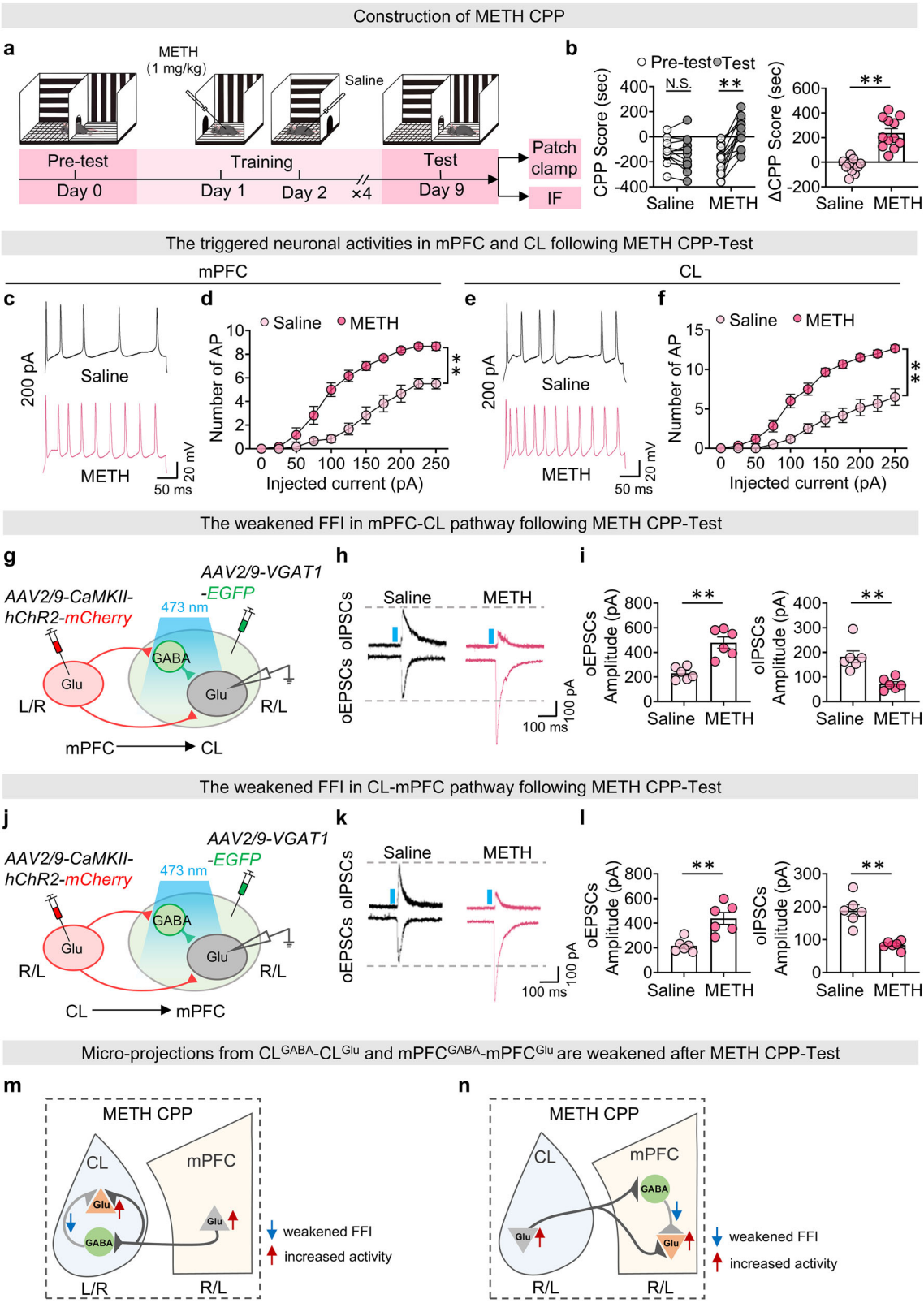

the right PFC is preferentially engaged during episodic memory retrieval[24]. Such specificity of the left and right hemispheres in memory encoding/retrieval is not absolute but rather involves mutual collaboration and dynamic changes. Studies have reported that the left and right hemispheres are interconnected by abundant nerve fiber pathways, such as the corpus callosum, enabling information communication and integration during memory-related processes[25]. These perspectives raise the intriguing possibility that the mPFC-CL interconnectivity might contribute to METH-related memory encoding and retrieval through hemisphere-specific manipulations.

The mPFC and CL are highly connected with a reciprocal connection pattern, suggesting a dynamic interplay that influences cognitive processing including reward memory[8,9,26]. The mPFC governs executive control over the decision-making, cognitive flexibility and

Fig. 5 | The mPFC^{Glu} and CL^{Glu} neurons are activated, while the FFI in mPFC-CL circuits is weakened under METH CPP. a Experimental design and timeline. **b** Analysis of CPP score (two-way ANOVA, $n = 12$, $F_{(1, 44)} = 14.2400$, $p = 0.0005$) and ΔCPP score (two-tailed unpaired t-test, $n = 12$, $t_{(22)} = 6.9100$, $p < 0.0001$). **c** Sample traces for the number of AP following current injection in mPFC. **d** The number of AP of mPFC neurons under whole-cell current-clamp configuration (two-way ANOVA, $n = 6$ cells from 4 mice, $F_{(10, 110)} = 7.1470$, $p < 0.0001$). **e** Same as (**c**) but in CL. **f** Same as (**d**) but in CL (two-way ANOVA, $n = 6$ cells from 4 mice, $F_{(10, 110)} = 8.4080$, $p < 0.0001$). **g** Schematic diagram of virus injection in the mPFC-CL pathway. **h** Representative traces showing the oEPSCs and oIPSCs in CL^{Glu} neurons. **i** Quantification of the amplitude showing the oEPSCs and oIPSCs in CL^{Glu} neurons. The amplitude of oEPSCs, two-tailed unpaired t-test, $n = 6$ cells from 4 mice, $t_{(10)} = 5.0150$, $p = 0.0005$. The amplitude of oIPSCs, two-tailed unpaired t-test, $n = 6$ cells from 4 mice, $t_{(10)} = 4.2780$, $p = 0.0016$. **j** Same as (**g**) but in the CL-mPFC pathway. **k** Same as (**h**) but in mPFC^{Glu} neurons. **l** Same as (**i**) but in mPFC^{Glu} neurons. The amplitude of oEPSCs, two-tailed unpaired t-test, $n = 6$ cells from 3 mice, $t_{(10)} = 4.1930$, $p = 0.0018$. The amplitude of oIPSCs, two-tailed unpaired t-test, $n = 6$ cells from 4 mice, $t_{(10)} = 5.6360$, $p = 0.0002$. **m**, **n** In the indirect pathway of the mPFC-CL interconnected circuit, the inhibitory effects of GABAergic interneurons on downstream Glu neurons were uniformly weakened in METH group mice after CPP test, leading to synchronous enhancement of mPFC^{Glu} and CL^{Glu} neuronal activities. All statistical tests are two-sided. Data presented as mean ± SEM. N.S., $p > 0.05$, $^{**}p < 0.01$. Source data are provided as a Source Data File.

reward[27,28]. In contrast, the CL has been proposed to act as a relay hub for the sensory integration and attention filter[29,30]. According to the hierarchical control rules in the brain, the top-down mPFC-CL pathway may play roles in regulation of sensory and limbic systems, while the bottom-up CL-mPFC pathway may relay information from subcortical regions to mPFC for higher-order cognitive processing. Our findings further suggest that the mPFC-CL circuits may constitute a functionally open-loop structure, rather than a fully closed feedback loop, making it particularly well-suited to supporting higher-order cognitive functions such as decision-making and memory formation. This open-loop configuration could facilitate iterative information processing, enabling flexible modulation and fine-tuning of neural signals during both memory encoding and retrieval[31]. Through reciprocal interactions, the mPFC and CL appear to jointly contribute to the integration of sensory, emotional, and cognitive inputs, ultimately promoting adaptive responses to complex environmental demands[32]. Such reentrant circuits enable precise modulation of cognitive and physiological functions via interregional feedback, contributing to the coordination and stability of complex behaviors[33]. For example, the hippocampus-mPFC loop integrates episodic memory with semantic and working memory systems, thereby enhancing the flexibility and accuracy of memory recall[34].

The encoding and retrieval processes of reward memory rely on the integration of sensory, cognitive, and emotional signals to form stable neural representations of experience[35]. The mPFC serves as a central executive top-down control[27,28]. It projects broadly to both cortical and subcortical regions to regulate cognitive flexibility, decision-making, and memory processing[27,28]. Among these projections, the CL has garnered attention for its role in attentional processing and sensory integration, which are essential for reinforcing drug-related cues[36,37]. Recent evidence suggests that projections from the mPFC to the CL are critically involved in regulating sensory and attentional processes. Consistent with our findings, Koga et al.[38] recently reported that mPFC neurons projecting to the contralateral CL preferentially respond to contralateral mechanical sensory stimulation, and these responses are enhanced during attentional engagement. In cognitively demanding tasks, the CL-projecting mPFC pathway appears to contribute to attentional selection and task engagement under demanding conditions. For instance, White et al.[39] reported that mPFC neurons projecting to the CL were activated during goal-directed learning tasks, and disruption of this pathway impaired the encoding of spatial rules. Further supporting this role, prior studies have demonstrated that inhibiting synaptic activity in the CL impairs the consolidation but not the acquisition or retrieval of an unconditioned memory formed in a nose-poke habituation task[40]. Collectively, these findings support the notion that the mPFC recruits the CL to filter and prioritize salient environmental cues during the formation of memory traces. However, other studies have emphasized the role of the PFC in retrieval processes. For example, during memory retrieval tasks in monkeys, the PFC has been shown to engage in bidirectional communication with the inferior temporal cortex (ITC) via theta-band activity[41], suggesting that the PFC also plays a vital role in the process of memory retrieval. These findings demonstrate that the interconnection between mPFC and CL plays crucial roles in reward memory.

Notably, the process of encoding and retrieval of reward memories require the coordinated activity across multiple brain regions. The hippocampus is essential for contextual memory encoding during the early phases of short-term memory formation[42,43], rapidly stabilizing environmental cues linked to reward or aversion[44,45]. By contrast, the mPFC plays a more prominent role in the regulation and retrieval of long-term contextual memories, as well as in the executive control of memory-guided behaviors[46]. Preston et al.[47] have reported that the progress of initial memory to stabilized ones become less dependent on the hippocampus, but rely much on neocortical networks. In the current study, we found that the mPFC-CL pathway is engaged in the encoding process of METH-related reward memory, indicating that the mPFC-CL pathway might coordinate with hippocampus to progressively assist subsequent cortical consolidation. As mentioned above, the mPFC-CL pathway might contribute to the selection and suppression of some cortical ensembles, thereby refining which of contextual associations become stabilized into long-term memory. In the future study, the role of network among hippocampus, mPFC and CL in the drug-related reward memory should be further explored.

In particular, the top-down mPFC-CL pathway seems to involve in the encoding process of METH-associated reward memory. We found that both mPFC^{Glu} neurons and CL^{Glu} neurons are activated during the training period of METH CPP, which is inconsistent with the above physiological rules between mPFC^{Glu} neurons and CL^{Glu} neurons: the activated Glu neurons at one end leading to suppressing the Glu neurons at the other end of connectivity between mPFC and CL. With the electrophysiological results, we found that FFI within CL along the top-down mPFC-CL pathway was weakened. Previous work has shown that cortical inputs to the CL evoke robust FFI within the CL[48], suggesting that the cortex not only excites but also exerts selective inhibitory control over claustral circuits through the recruitment of local interneurons. In this study, we identified both a direct mPFC^{Glu}-CL^{Glu} excitatory pathway and an indirect mPFC^{Glu}-CL^{GABA}-CL^{Glu} inhibitory pathway, which together may gate cortico-claustral transmission by balancing excitation and inhibition. We also found that activation of mPFC could suppress CL under normal condition, while both mPFC and CL were activated after METH CPP in male mice. These results suggest that METH may reduce inhibitory tone of CL^{GABA} neurons on CL^{Glu} neurons, resulting in both mPFC and CL run toward excessive excitation. This mechanism may explain why individuals with METH addiction tend to overvalue drug-related rewards while discounting negative consequences. Notably, we found that during CPP-Training rather than during CPP-Test, chemogenetic activation of CL^{GABA} neurons on the mPFC^{Glu}-CL^{GABA}-CL^{Glu} pathway which restores the FFI of local CL^{GABA} -CL^{Glu} microcircuit, or suppressing mPFC^{Glu} neurons that projecting to CL^{Glu} neurons, could block the acquisition of METH CPP. These findings underscore the critical role of the mPFC-CL pathway in METH reward learning and cue-driven memory consolidation, particularly through the weakened FFI in the mPFC^{Glu}-CL^{GABA}-CL^{Glu} pathways.

https://doi.org/10.1038/s41467-025-68009-4

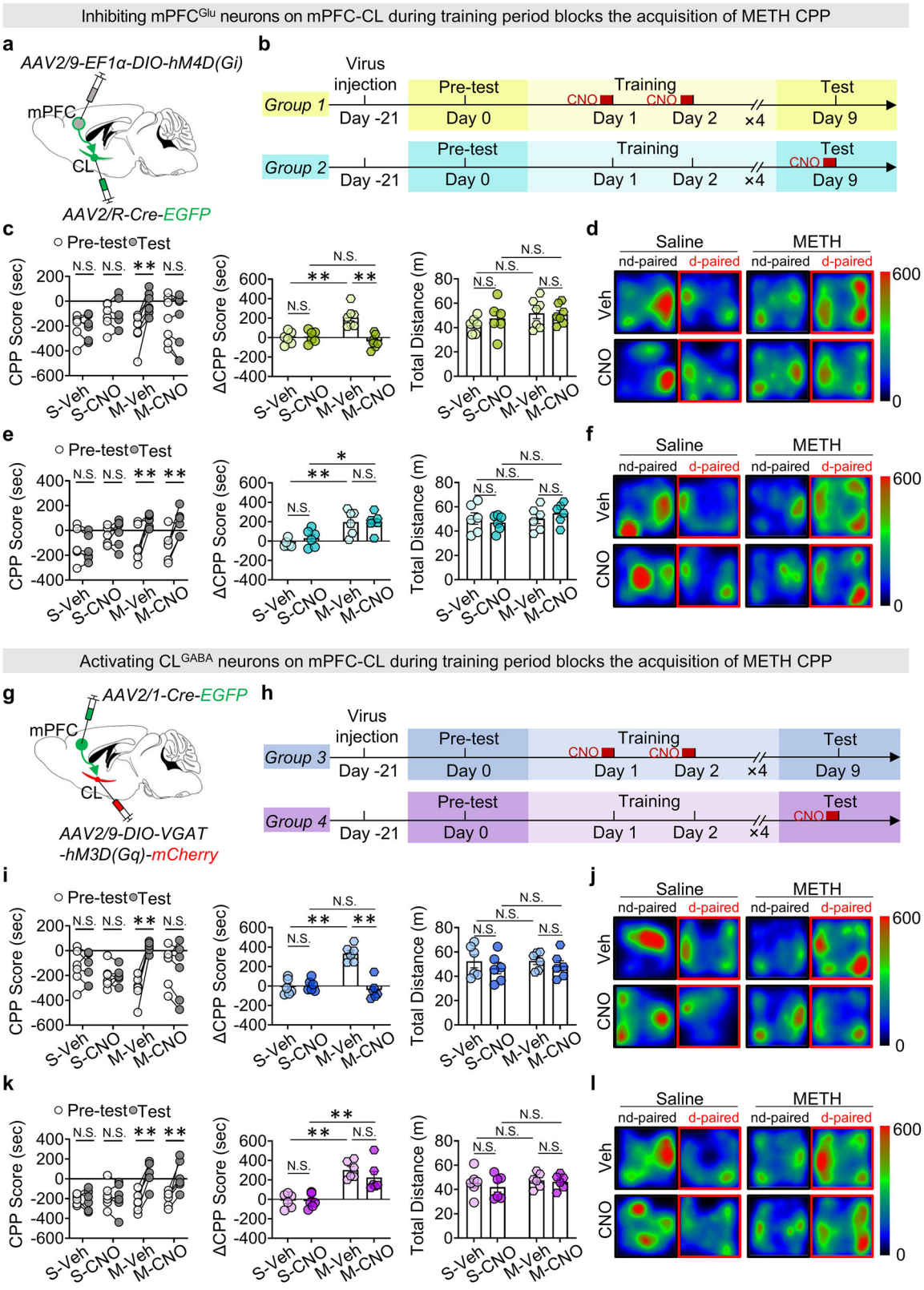

By contrast, the bottom-up pathway of CL-mPFC appears to be involved in the retrieval of METH reward memory. Here, unlike the above physiological rules between mPFC^{Glu} neurons and CL^{Glu} neurons, we found that both mPFC^{Glu} neurons and CL^{Glu} neurons are activated following METH CPP-Test by METH-paired environmental context. Electrophysiological studies demonstrate that CL inputs predominantly induce strong and widespread FFI in the PFC under physiological conditions, largely via parvalbumin (PV^{+}) and neuropeptide Y (NPY^{+}) interneurons[22]. This inhibitory control ensures precise regulation of prefrontal excitability and prevents runaway excitation. We speculate that METH disrupts this inhibitory brake by impairing the indirect CL^{Glu}-mPFC^{GABA}-mPFC^{Glu} inhibitory pathway, ultimately weakening the inhibitory regulation of mPFC outputs. Notably, we found that during CPP-Test rather than during

Fig. 6 | The top-down mPFC-CL pathway contributes to the encoding of METH reward memory during the process of METH CPP-Training. a Schematic diagram of virus injection in mPFC and CL. **b** Experiment timeline. **c** Analysis of CPP score (two-way ANOVA, $n = 6–7$, $F_{(3, 22)} = 14.4300$, $p < 0.0001$), ΔCPP score (two-way ANOVA, $n = 6–7$, $F_{(1, 22)} = 18.5700$, $p = 0.0003$) and total distance (two-way ANOVA, $n = 6–7$, $F_{(1, 22)} = 0.5959$, $p = 0.4483$) in CPP apparatus of Group 1 mice. **d** Heatmap of Group 1 mice. **e** Analysis of CPP score (two-way ANOVA, $n = 6$, $F_{(3, 20)} = 7.7760$, $p = 0.0012$), ΔCPP score (two-way ANOVA, $n = 6$, $F_{(1, 20)} = 0.5947$, $p = 0.4496$) and total distance (two-way ANOVA, $n = 6$, $F_{(1, 20)} = 1.0930$, $p = 0.3083$) in CPP apparatus of Group 2 mice. **f** Heatmap of Group 2 mice. **g** Schematic diagram of virus injection in mPFC and CL. **h** Experiment timeline. **i** Analysis of CPP score (two-way ANOVA, $n = 6$, $F_{(3, 20)} = 27.5100$, $p < 0.0001$), ΔCPP score (two-way ANOVA, $n = 6$, $F_{(1, 20)} = 34.3700$, $p < 0.0001$) and total distance (two-way ANOVA, $n = 6$, $F_{(1, 20)} = 0.0303$, $p = 0.8636$) in CPP apparatus of Group 3 mice. **j** Heatmap of Group 3 mice. **k** Analysis of CPP score (two-way ANOVA, $n = 6$, $F_{(3, 20)} = 15.4100$, $p < 0.0001$), ΔCPP score (two-way ANOVA, $n = 6$, $F_{(1, 20)} = 0.7596$, $p = 0.3938$) and total distance (two-way ANOVA, $n = 6$, $F_{(1, 20)} = 0.1264$, $p = 0.7259$) in CPP apparatus of Group 4 mice. **l** Heatmap of Group 4 mice. All statistical tests are two-sided. Data presented as mean ± SEM. N.S., $p > 0.05$, $^{*}p < 0.05$, $^{**}p < 0.01$. Source data are provided as a Source Data File. The mouse brain and anatomical structures of **a** and **g** were drawn according to "The Mouse Brain in Stereotaxic Coordinates Third Edition (Keith B.J. Franklin & George Paxinos)".

CPP-Training, chemogenetic activation of $mPFC^{GABA}$ neurons on the CL^{Glu}-$mPFC^{GABA}$-$mPFC^{Glu}$ pathway which restores the FFI of local $mPFC^{GABA}$ -$mPFC^{Glu}$ microcircuit, or suppressing CL^{Glu} neurons that projecting to $mPFC^{Glu}$ neurons, could block the acquisition of METH CPP, suggesting that suppressing mPFC excitability during memory recall by triggering its indirect inhibitory pathways or inhibiting its direct excitatory pathways from CL to mPFC could reduce the selective retrieval of METH-associated environmental cues. The CL functions as a key integrative hub for reward processing and multisensory transmission, with widespread projections to the cortex[22,49]. Recent studies have emphasized the functional relevance of CL projections to the prefrontal and frontal cortices in mediating cognitive tasks drug-associated memories[8,9,22]. Jackson et al.[22] demonstrated that CL provides potent inhibitory input to the PFC which is enough to silence ongoing neural activity and modulate cognitive performance. Additionally, the CL acts as a gatekeeper for context-relevant information by modulating frontal cortical activity to enhance attention[50]. Furthermore, silencing CL neurons projecting to the mPFC has been reported to attenuate METH-induced impulsive behavior in rats[51]. Inconsistent with our results, Terem et al.[9] demonstrated that inhibition of dopamine receptor D1 (D1R)-positive CL neurons that projecting to frontal cortex impaired the formation of cocaine but not retrieval. Although both studies implicate the bottom-up CL-mPFC pathway, differences in neuronal populations and drug-specific mechanisms may account for the discrepancies. However, all these findings support the idea that the CL integrates motivationally salient stimuli and facilitates their retrieval via the modulation of frontal and prefrontal circuits.

METH exposure is known to remodel the E/I balance by impairing the interneurons' excitability[52]. Here, we found that weakened FFI, caused by impaired local interneurons within the indirect pathways of mPFC-CL circuits, represents a key mechanism underlying METH-induced CPP. The reduction in inhibitory gating of CL^{Glu} neurons by CL^{GABA} interneurons likely impairs the CL's ability to filter cortical inputs, leading to excessive propagation of excitatory signals. In turn, weakened CL-driven FFI on $mPFC^{GABA}$-$mPFC^{Glu}$ would diminish inhibitory control over prefrontal outputs, amplifying excitatory drive during the retrieval of drug-associated memories. This bidirectional breakdown in mPFC-CL circuits could reinforce drug cues and impair cognitive flexibility, which contribute to the persistence of maladaptive drug-context associations. Besides, we also found that the weakened FFI in the top-down mPFC-CL pathway and in the bottom-up CL-mPFC pathway may contribute to different stages of METH-induced reward memory. Specifically, disinhibition of FFI of $mPFC^{GABA}$ neurons on $mPFC^{Glu}$ neurons could rescue the retrieval of METH reward memory instead of encoding phase of METH-context association. Conversely, strengthen of FFI of CL^{GABA} neurons on CL^{Glu} neurons suppress the initial formation of METH reward memory rather than the retrieval phase. This phenomenon may be associated with the reciprocal architecture between mPFC and CL, which recruiting different patterns of information communication and integration in the brain. Overall, the mPFC-CL circuits contribute to integrate drug-associated contextual memories in a pathway-specific manner, potentially facilitating their persistence and retrieval during METH-related behaviors. In the future, several lines of investigation may clarify the role of FFI attenuation in METH CPP. First, cell-type-specific approaches are needed to determine whether PV^{+} neurons, somatostatin (SOM^{+}) neurons, vasoactive intestinal peptide (VIP^{+}) neurons and NPY^{+} neurons are preferentially affected in the CL and mPFC. Second, molecular analyses of GABA release and GABA receptor subunits at inhibitory synapses may help identify pharmacological entry points.

There are some limitations in the current study. First, there is lack of female mouse model, partly due to the known effects of the estrous cycle and hormonal fluctuations on neuronal excitability and behavioral outcomes[53–55]. Previous human and animal studies have shown that females are more susceptible to developing and maintaining addiction as well as relapse induction compared to males, and these sex differences are largely attributed to the modulatory effects of estrogen on the dopaminergic system[56,57]. In the current study, we only used male mice to explore the role of mPFC-CL circuits in METH-related reward memory. Whether similar neural and behavioral mechanisms occur in female mice remains to be determined, and this issue will be an important focus of future research. Second, our study did not distinguish GABAergic interneuron subtypes within the mPFC-CL circuits, despite emerging evidence suggesting substantial functional heterogeneity among them[58–60]. In mPFC, GABAergic neurons include PV^{+} neurons, SOM^{+} neurons, VIP^{+} neurons and NPY^{+} neurons. Specifically, PV^{+} and NPY^{+} neurons are thought to be central to FFI[22,49,61]. In CL, GABAergic neurons are predominantly divided into PV^{+} and SOM^{+} neurons subtypes[18], with PV^{+} neurons likely playing a crucial role in FFI[17,49].

In summary, we identified two relatively independent pathways connecting the mPFC and CL: the top-down mPFC-CL pathway and the bottom-up CL-mPFC pathway, each comprising both direct excitatory and indirect inhibitory projections. The mPFC-CL pathway primarily mediates inter-hemispheric communication, while the CL-mPFC pathway mainly supports intra-hemispheric connections. The minimal overlap between Glu input and output neurons within each region suggests an open-loop circuit architecture. Under physiological conditions, the local $mPFC^{GABA}$ or CL^{GABA} interneurons exert a robust FFI on the $mPFC^{Glu}$ or CL^{Glu} neurons along the indirect inhibitory pathways between mPFC and CL. Under the METH CPP model, the top-down mPFC-CL pathway is involved in the encoding process of METH reward memory, while the bottom-up CL-mPFC pathway contributes to the retrieval of METH reward memory. The FFI mediated by GABAergic interneurons on the Glu neurons along the reciprocal connections between mPFC and CL might be a promising intervention target for blocking the METH reward memory.

Methods

Animals

Male C57BL/6 wild-type (WT) mice (6 - 8 weeks of age, 20 - 24 g) were used (Changzhou Cavens Experimental Animal Co., China).

https://doi.org/10.1038/s41467-025-68009-4

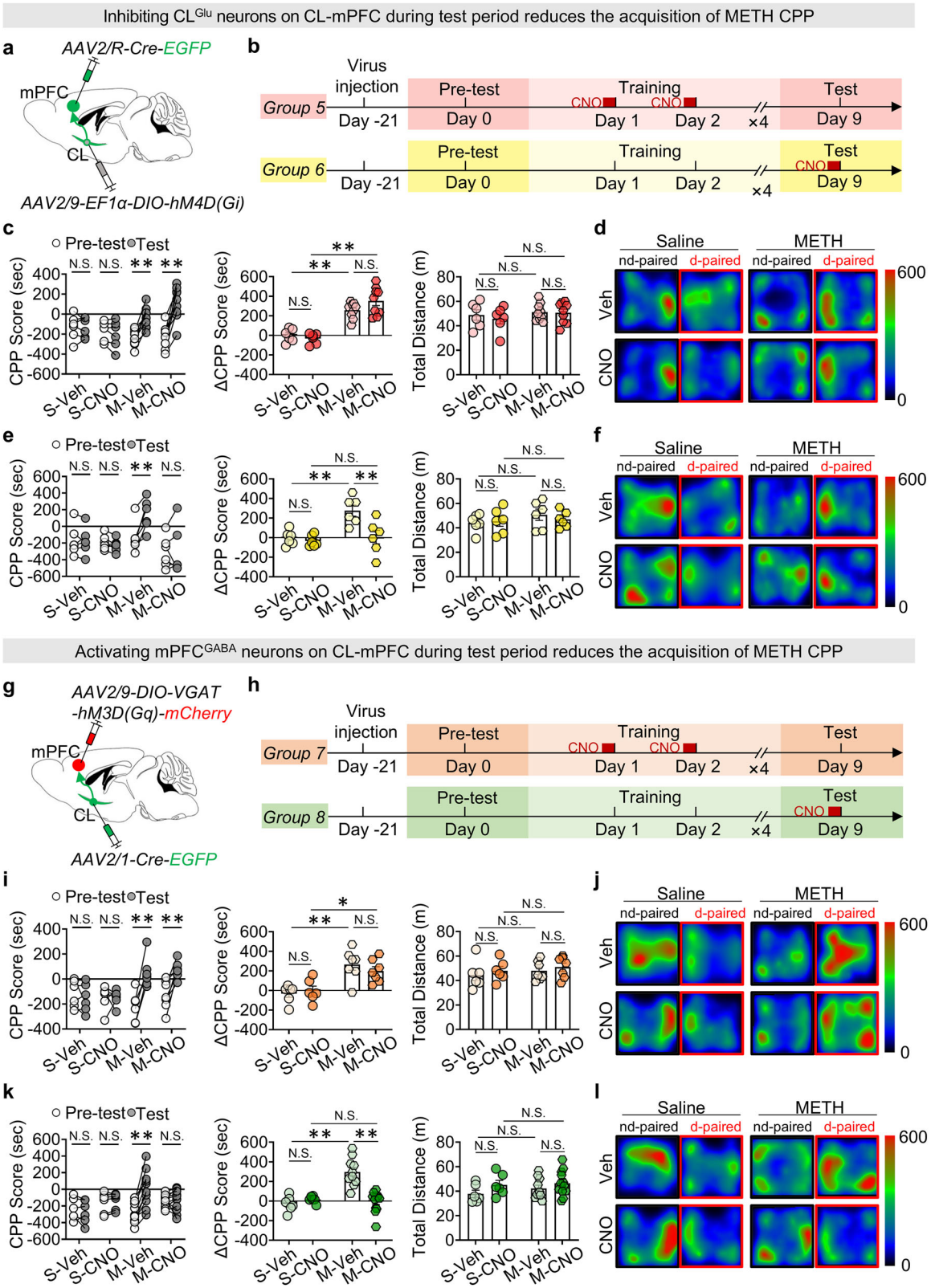

All mice were housed under controlled conditions with constant temperature (24 ± 2 °C) and humidity (50 ± 10%) with a 12-h light/dark cycle (lights on at 8 a.m.) and allowed free access to food and water in their homecages. All procedures were carried out following the National Institutes of Health Guide for the Care and Use of Laboratory Animals and approved by the Institutional Animal Care and Use Committee (IACUC) at Nanjing University of Chinese Medicine, China.

Stereotaxic surgery

Male mice were anesthetized with 2% isoflurane (RWD, China), placed on a stereotaxic apparatus (RWD, China), and their skulls were clamped on both sides of the ears to stabilize the brain. After disinfecting the scalps with iodine tincture followed by 70% medical alcohol, the scalps were incised to expose the skull. A 30% hydrogen peroxide solution was applied to the skull to dissolve the connective

Fig. 7 | The bottom-up CL-mPFC pathway contributes to the retrieval of METH reward memory during the process of METH CPP-Test. a Schematic diagram of virus injection in CL and mPFC. **b** Experiment timeline. **c** Analysis of CPP score (two-way ANOVA, $n = 6–9$, $F_{(3, 26)} = 20.6900$, $p < 0.0001$), ΔCPP score (two-way ANOVA, $n = 6–9$, $F_{(1, 26)} = 2.9490$, $p = 0.0978$) and total distance (two-way ANOVA, $n = 6–9$, $F_{(1, 26)} = 0.1642$, $p = 0.6887$) in CPP apparatus of Group 5 mice. **d** Heatmap of Group 5 mice. **e** Analysis of CPP score (two-way ANOVA, $n = 6$, $F_{(3, 20)} = 8.7980$, $p = 0.0006$), ΔCPP score (two-way ANOVA, $n = 6$, $F_{(1, 20)} = 6.1340$, $p = 0.0223$) and total distance (two-way ANOVA, $n = 6$, $F_{(1, 20)} = 0.4733$, $p = 0.4994$) in CPP apparatus of Group 6 mice. **f** Heatmap of Group 6 mice. **g** Schematic diagram of virus injection in CL and mPFC. **h** Experiment timeline. **i** Analysis of CPP score (two-way ANOVA, $n = 6–7$, $F_{(3, 22)} = 9.1630$, $p = 0.0004$), ΔCPP score (two-way ANOVA, $n = 6–7$, $F_{(1, 22)} = 0.9862$, $p = 0.3315$) and total distance (two-way ANOVA, $n = 6–7$, $F_{(1, 22)} = 0.0020$, $p = 0.9649$) in CPP apparatus of Group 7 mice. **j** Heatmap of Group 7 mice. **k** Analysis of CPP score (two-way ANOVA, $n = 6–12$, $F_{(3, 30)} = 18.8200$, $p < 0.0001$), ΔCPP score (two-way ANOVA, $n = 6–12$, $F_{(1, 30)} = 20.5300$, $p < 0.0001$) and total distance (two-way ANOVA, $n = 6–12$, $F_{(1, 30)} = 0.2072$, $p = 0.6523$) in CPP apparatus of Group 8 mice. **l** Heatmap of Group 8 mice. All statistical tests are two-sided. Data presented as mean ± SEM. N.S., $p > 0.05$, $^{*}p < 0.05$, $^{**}p < 0.01$. Source data are provided as a Source Data File. The mouse brain and anatomical structures of **a** and **g** were drawn according to "The Mouse Brain in Stereotaxic Coordinates Third Edition (Keith B.J. Franklin & George Paxinos)".

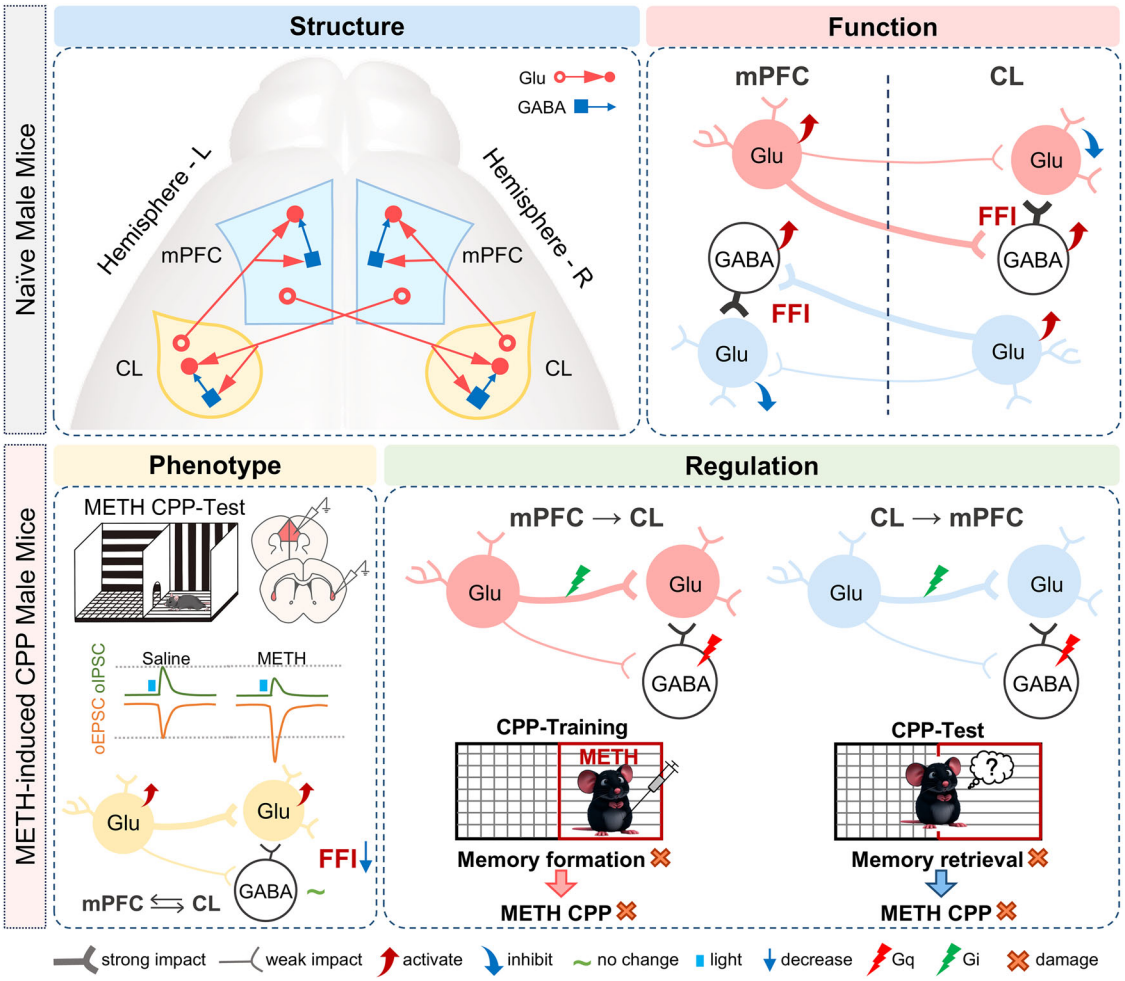

Fig. 8 | Schematic summary of present study. There is a hemisphere-specific reciprocal projection relationship between the mPFC and CL: the top-down mPFC-CL pathway which primarily facilitates communication between the left and right hemispheres of the brain, as well as the bottom-up CL-mPFC pathway that predominantly connects regions within the ipsilateral hemisphere. The projecting Glu neurons are rarely overlapped with the receiving Glu neurons in each region of connectivity pathways between mPFC and CL, which are connected anterogradely to form an unclosed circuit. There are both direct excitatory and indirect inhibitory projection patterns, forming Glu-Glu pathways and Glu-GABA-Glu pathways in mPFC-CL circuits. Under physiological conditions, the local $mPFC^{GABA}$ or CL^{GABA} interneurons exert a robust FFI on the $mPFC^{Glu}$ or CL^{Glu} neurons along the indirect inhibitory pathways between mPFC and CL. However, under the METH CPP model, both $mPFC^{Glu}$ and CL^{Glu} neurons are activated in mice, due to the weakened FFI of GABAergic neurons on the indirect inhibitory pathways between mPFC and CL. The top-down mPFC-CL pathway involves the encoding process of METH-related context memory which was established during CPP-Training, while bottom-up CL-mPFC pathway contributes to the retrieval of METH-related context memory which carried out when CPP-Test.

tissue, and then microsurgical procedures were initiated. Small holes with a diameter of approximately 1 millimeter were drilled in the skull of the mice to facilitate virus injection or optical fiber implantation. For virus injections, a volume of 200 nL or 50 nL per side was injected into mPFC or CL, respectively. Injections were given over 5 min at a rate of 20 nL/min by an infusion pump (RWD, China) and left in place for 10 min after the procedure. Stereotaxic coordinates were defined as anterior-posterior (AP) from the bregma, mediolateral (ML) from the midline and dorsal-ventral (DV) from the brain surface. The coordinates utilized in this study were as follows, mPFC (AP, +1.94 mm; ML, ±0.4 mm; DV, −2.5 mm), CL (AP, +0.98 mm; ML, ±2.85 mm; DV, −3.85 mm).

Neuron labeling and virus tracing

All viruses utilized in the present study were packaged by BrainVTA (China). For anterograde tracing, the rAAV2/9-hSyn-EGFP-WPRE-hGH pA (PT-1990, 5.24E + 12 vg/mL, BrainVTA, China) was unilaterally injected into mPFC or CL of WT mice. For retrograde tracing, the rAAV2/Retro-hSyn-mCherry-WPRE-hGH pA (PT-0100, 5.30E + 12 vg/mL, BrainVTA, China) was unilaterally injected into CL or mPFC of WT mice. In order to identify the types of neurons in mPFC that project to CL, the rAAV2/Retro-hSyn-mCherry-WPRE-hGH pA (PT-0100, 5.30E + 12 vg/mL, BrainVTA, China) was unilaterally injected into CL. To identify the types of neurons in mPFC that receive projections from the upstream CL, trans-synaptic anterograde virus rAAV2/1-hSyn-CRE-WPRE-hGH pA (PT-0136, 1.09E + 13 vg/mL, BrainVTA, China) was unilaterally injected into CL combined with Cre-dependent virus rAAV2/9-hSyn-DIO-EGFP-WPRE-hGH pA (PT-1103, 5.04E + 12 vg/mL, BrainVTA, China) in mPFC. Similarly, in order to identify the types of neurons in CL that project to mPFC, the rAAV2/Retro-hSyn-mCherry-WPRE-hGH pA (PT-0100, 5.30E + 12 vg/mL, BrainVTA, China) was unilaterally injected into mPFC. To identify the types of neurons in CL that receive projections from the upstream mPFC, trans-synaptic anterograde virus rAAV2/1-hSyn-CRE-WPRE-hGH pA (PT-0136, 1.09E + 13 vg/mL, BrainVTA, China) was unilaterally injected into mPFC combined with Cre-dependent virus rAAV2/9-hSyn-DIO-EGFP-WPRE-hGH pA (PT-1103, 5.04E + 12 vg/mL, BrainVTA, China) in CL.

Immunofluorescence

Male mice were deeply anesthetized with isoflurane (RWD, China) and sequentially perfused with 0.9% saline and 4% paraformaldehyde (PFA). The brains were removed and post-fixed in 4% PFA at 4 °C overnight, then transferred to 30% (w/v) sucrose. The coronal brain sections (30 μm) were continuously sectioned by a cryostat freezing microtome (Leica, Germany) and used for immune-fluorescence. The sections were washed in phosphate-buffered saline (PBS) 3 times (10 min each time) and incubated in 0.3% (v/v) Triton X-100 for 30 min. Then, they were blocked with 5% donkey serum for 90 min at room temperature, and incubated overnight at 4 °C with the following primary antibodies: rabbit anti-c-Fos (1:2000, RRID: AB_2247211, Cell Signaling Technology, USA), guinea pig anti-c-Fos (1:3000, RRID: AB_2905595, Synaptic system, Germany), rabbit anti-CaMKII (1:500, RRID: AB_305050, Abcam, UK), rabbit anti-CaMKII (1:500, RRID: AB_2887447, GeneTex, USA), mouse anti-GAD67 (1:500, RRID: AB_2938602, Millipore, USA) followed by the corresponding fluorophore-conjugated secondary antibodies for 90 min at room temperature. CaMKII and GAD67 were used to label Glu and GABA neurons, respectively. The following secondary antibodies were used: Alexa Fluor 555-labeled donkey anti-rabbit secondary antibody (1:500, RRID: AB_162543, Invitrogen, USA), Alexa Fluor 488-labeled donkey anti-rabbit (1:500, RRID: AB_2762833, Invitrogen, USA), Alexa Fluor 555-labeled donkey anti-mouse secondary antibody (1:500, RRID: AB_2762848, Invitrogen, USA), Alexa Fluor 488-labeled donkey anti-mouse secondary antibody (1:500, RRID: AB_141607, Invitrogen, USA), Alexa Fluor 680-labeled donkey anti-rabbit secondary antibody (1:500, RRID: AB_2762836, Invitrogen, USA), Alexa Fluor 680-labeled donkey anti-mouse secondary antibody (1:500, RRID: AB_2762831, Invitrogen, USA), Alexa Fluor 488-labeled donkey anti-guinea pig (1:500, RRID: AB_2736871, Abcam, UK), Alexa Fluor 555-labeled donkey anti-guinea pig (1:500, RRID: AB_3099754, Abcam, UK). Fluorescence signals were visualized using either the Leica DM8I THUNDER Imager 3D Tissue microscope (Leica, Germany) or the Leica TCS SP8 Laser Scanning Confocal microscope (Leica, Germany).

Fluorescence micro-optical section tomography (fMOST)

For fMOST imaging, the rAAV2/9-hSyn-EGFP-WPRE-hGH pA (PT-1990, 5.24E + 12 vg/mL, BrainVTA, China) was unilaterally injected into CL and the rAAV2/9-hSyn-mCherry-WPRE-hGH pA (PT-0100, 5.61E + 12 vg/mL, BrainVTA, China) was unilaterally injected into mPFC. Three weeks later, male mice were perfused with PBS followed by 4% PFA and brains were dissected and post-fixed in 4% PFA for 24 h at 4 °C. After fixation, the brains were rinsed overnight at 4 °C in 0.01 M PBS and subsequently dehydrated in a graded ethanol series (25%, 50%, 70% and 100%, 2 h at each concentration) at 4 °C. After dehydration, dehydrated brains were put in a brown bottle and infiltrated with 100% LR White mixed with Sudan black B (SBB) Resin (BE-L6-05, OEBio, China) for 9 h. Finally, BioMolding LR White Embedding Kit (BE-L6-05, OEBio, China) was used to polymerize and the special samples were placed in a constant temperature drying chamber at 37.5 °C for 24 h. The embedded brains were imaged under an fMOST microscope (BioMapping 5000 N, OEBio, China) at a voxel resolution of 0.3 × 0.3 × 2 μm. The collected images were processed using Imaris Viewer software (version 9.0, Oxford Instruments, UK).

Fiber photometry

Under physiological conditions, a mixture of the rAAV2/9-EF1α-DIO-hM3D(Gq)-WPRE-hGH pA (PT-2958, 6.53E + 12 vg/mL, BrainVTA, China) and the rAAV2/9-hSyn-CRE-WPRE-hGH pA (PT-0136, 5.27E + 12 vg/mL, BrainVTA, China) was bilaterally injected into mPFC or CL of WT mice. After 2 weeks of expression, the rAAV2/1-hSyn-CRE-WPRE-hGH pA (PT-0136, 1.09E + 13 vg/mL, BrainVTA, China) was bilaterally injected into the mPFC or CL, while the rAAV2/9-VGAT1-DIO-GCaMp6s-WPRE-hGH pA (PT-6173, 5.27E + 12 vg/ml, BrainVTA, China) and rAAV2/9-CaMKII-DIO-jRGECO1a-WPRE-hGH pA (PT-2948, 5.32E + 12 vg/ml, BrainVTA, China) were bilaterally injected into CL or mPFC. Under pathological conditions, the rAAV2/1-hSyn-CRE-WPRE-hGH pA (PT-0136, 1.09E + 13 vg/mL, BrainVTA, China) was bilaterally injected into the mPFC or CL, while the rAAV2/9-VGAT1-DIO-GCaMp6s-WPRE-hGH pA (PT-6173, 5.27E + 12 vg/ml, BrainVTA, China) was bilaterally injected into CL or mPFC. An optical fiber (200 μm outer diameter, 0.37 numerical aperture, Thinkerbiotech, China) was placed 100 μm above the viral injection site. After 3 weeks, the calcium-dependent fluorescence signals in mPFC or CL were recorded at their homecages. The calcium-dependent fluorescence signals were obtained by stimulating cells that transfected with the GCaMp6s virus or jRGECO1a virus using a 473 nm LED or 593 nm LED, while calcium-independent signals were obtained by stimulating these cells with a 405 nm LED. The LED lights of 473 nm, 593 nm and 405 nm were alternated at 40 fps and light emission was recorded using sCMOS camera containing the entire fiber bundle (2 m in length, NA = 0.37, 200 μm core, Thinkerbiotech, China). The analog voltage fluorescent signals were filtered at 30 Hz and digitized at 100 Hz. The signals were recorded and analyzed by ThinkerTech TripleColor MultiChannel fiber photometry Acquisition Software and fiber photometry Analysis Package (Thinkerbiotech, China). For the physiological conditions, F0 is the baseline fluorescence signal which was recorded for 5 min with 0.5-min record and 4.5-min interval (1 session) prior to Clozapine-N-oxide (CNO) treatment. F is the real-time fluorescence signal which was recorded for 60 min with a 0.5-min recording and 4.5-min interval (11 sessions). For the pathological conditions, F0 is the baseline fluorescence signal which was recorded for 0.5 min in homecages. F is the real-time fluorescence signal which was recorded for 15 min in the CPP apparatus. For each session, the photometry signal F was converted to $\Delta F/F$ by calculating $\Delta F/F\ (\%) = (F - F0)/F0 \times 100\%$. The raw heatmap data from one mouse was merged as a statistical point and normalized using area under the curve (AUC) normalization. The AUC represented the integral under the recording duration relative to the corresponding baseline at each trial.

Acute brain slice preparation

Male mice were deeply anesthetized with isoflurane (RWD, China) and perfused with ice-cold cutting solution (in mM: 92 N-methyl-D-glutamine, 2.5 KCl, 1.2 NaH_2PO_4, 30 $NaHCO_3$, 20 HEPES, 0.5 $CaCl_2$, 10

$MgSO_4$, 25 glucose, 5 sodium ascorbate, 2 thiourea, and 3 sodium pyruvate, pH adjusted to 7.3 with HCl, osmolarity 305, and saturated with 95% O_2/5% CO_2). Slices containing the mPFC or CL were cut at a 200 μm thickness using a vibratome in 4 °C cutting solution. The slices were transferred to 37 °C cutting solution and kept for ~9 min, then transferred to oxygenated holding solution (in mM: 86 NaCl, 2.5 KCl, 1.2 NaH_2PO_4, 35 $NaHCO_3$, 20 HEPES, 2 $CaCl_2$, 1 $MgSO_4$, 25 glucose, 5 sodium ascorbate, 2 thiourea, and 33 sodium pyruvate, pH adjusted to 7.3, osmolarity 305, and saturated with 95% O_2/5% CO_2) to allow for recovery at room temperature for at least 60 min before recordings. During electrophysiological recordings, the brain slices were continuously perfused with oxygenated artificial CSF (ACSF, in mM: 119 NaCl, 2.5 KCl, 1 NaH_2PO_4, 1.3 $MgCl_2$, 2.5 $CaCl_2$, 26.2 $NaHCO_3$, and 11 glucose, osmolarity 290, saturated with 95% O_2/5% CO_2) and maintained at 31 °C by a solution heater (TC-324C, Warner Instruments, USA).

Whole-cell recordings

Whole-cell voltage-clamp microelectrodes (3–5 MΩ) were filled with Cs^+-based internal solution (in mM: 130 $CsMeSO_4$, 10 NaCl, 10 EGTA, 4 Mg-ATP, 0.3 Na-GTP, 10 HEPES, pH 7.25–7.30; osmolarity 290). Excitatory postsynaptic currents (EPSCs) were recorded at a holding potential of −70 mV and inhibitory postsynaptic currents (IPSCs) were recorded at a holding potential of +10 mV. A blue light laser was coupled to the stimulator to deliver optostimulation. Optically-evoked EPSCs (oEPSCs) or IPSCs (oIPSCs) were recorded by delivering a 20 Hz pulse train of a 3–5 mW blue laser (473 nm) through an optic fiber which was held upon the target area.

To verify the synaptic connectivity between mPFC and CL, the rAAV2/9-CaMKII-hChR2(H134R)-mCherry-WPRE-hGH pA (PT-0297, 4.78E + 12 vg/mL, BrainVTA, China) was bilaterally injected into mPFC and the rAAV2/9-VGAT1-EGFP-WPRE-hGH pA (PT-3176, 5.31E + 12 vg/mL, BrainVTA, China) was bilaterally injected into CL. CaMKII-positive neurons in mPFC were identified by mCherry and GABA-positive neurons in CL were identified by EGFP. To verify the synaptic connectivity between CL and mPFC, the rAAV2/9-CaMKII-hChR2(H134R)-mCherry-WPRE-hGH pA (PT-0297, 4.78E + 12 vg/mL, BrainVTA, China) was bilaterally injected into CL and the rAAV2/9-VGAT1-EGFP-WPRE-hGH pA (PT-3176, 5.31E + 12 vg/mL, BrainVTA, China) was bilaterally injected into mPFC. CaMKII-positive neurons in CL were identified by mCherry and GABA-positive neurons in mPFC were identified by EGFP.

To verify the functional connections of the microcircuits in the mPFC, the rAAV2/1-hSyn-CRE-WPRE-hGH pA (PT-0136, 1.90E + 13 vg/mL, BrainVTA, China) was bilaterally injected into CL and the rAAV2/9-VGAT1-DIO-hChR2(H134R)-EYFP-WPRE-hGH pA (PT-4270, 5.13E + 12 vg/mL, BrainVTA, China) was bilaterally injected into mPFC. GABA-positive neurons in mPFC were identified by EYFP. To verify the functional connections of the microcircuits in the CL, the rAAV2/1-hSyn-CRE-WPRE-hGH pA (PT-0136, 1.90E + 13 vg/mL, BrainVTA, China) was bilaterally injected into mPFC and the rAAV2/9-VGAT1-DIO-hChR2(H134R)-EYFP-WPRE-hGH pA (PT-4270, 5.13E + 12 vg/mL, BrainVTA, China) was bilaterally injected into CL. GABA-positive neurons in CL were identified by EYFP.

To examine synaptic specificity, the oEPSCs or oIPSCs were recorded from GABA-positive or CaMKII-positive neurons in voltage clamp. Tetrodotoxin (TTX, sodium channel blocker, 1 μM) and 4-aminopyridine (4-AP, potassium channel blocker, 100 μM) were used in the recording ACSF solution to verify whether the light evoked currents were monosynaptic. Picrotoxin (PTX, GABA receptor antagonist, 100 μM), 2,3-Dihydroxy-6-nitro-7-sulfamoyl-benzo (f) quinoxaline (NBQX, AMPA receptor antagonist, 10 μM) and D-2-Amino-5-phosphonovaleric acid (AP5, NMDA receptor antagonist, 20 μM) were used in the recording ACSF solution to verify neuron-specific connections.

All the light stimulations were applied through QAXK-LASER-473 nm (ThinkerTech, China). All signals were filtered at 4 kHz, amplified at 5 × using a MultiClamp 700B amplifier (Molecular Devices, USA) and digitized at 10 kHz with a Digidata 1550B analog-to-digital converter (Molecular Devices, USA). All data were analyzed with Clampfit 10.6 software (Molecular Devices, USA).

Conditioned place preference (CPP)

The conditioned place preference (CPP) test was conducted using a standard two-chambered apparatus equipped with two conditioning compartments, which differed in their patterns (horizontal stripes and vertical stripes) and floors (bar and grid). The experimental paradigm of CPP consisted of three phases: the pre-conditioning test (Baseline/Pre-Test, day 0), conditioning (CPP-Training, day 1–8), and post-conditioning test (CPP-Test, day 9). The mice were habituated to the apparatus 2 days prior to pre-conditioning for 45 min per day. Baseline preference was determined by allowing mice to freely explore both chambers of the CPP apparatus for 15 min. An initial measurement of baseline preference was assessed by recording the time spent in each chamber. Based on initial chamber preference, the non-preferred chamber was designated as the drug-paired chamber, and the preferred chamber was designated as the non-drug-paired chamber. CPP-Training was confined to a non-drug-paired chamber paired with a saline (0.2 mL, i.p.) injection on even days and to a drug-paired chamber paired with METH (1 mg/kg, i.p., China Institute for Food and Drug Control) injection on odd days. After each injection, the male mice were confined to the corresponding chamber (non-drug-paired chamber or drug-paired chamber) for 45 min. During CPP-Test, mice were again placed in the chamber of the CPP apparatus and allowed to explore the two chambers freely without any drug treatment for 15 min.

The CPP score was defined as the time spent in the drug-paired chamber (T_{drug}) minus the time spent in the non-drug (used saline as control in the current study)-paired chamber ($T_{non\text{-}drug}$) during a given session (Pre-Test or CPP-Test), i.e., CPP score = $T_{drug} - T_{non\text{-}drug}$. The ΔCPP score was calculated as the CPP score of CPP-Test minus the CPP score of Pre-Test, i.e., ΔCPP score = $(T_{drug} - T_{non\text{-}drug})_{CPP\text{-}Test} - (T_{drug} - T_{non\text{-}drug})_{Pre\text{-}Test}$. Generally, METH strongly reversed preference and resulted in a positive CPP score, and the CPP score was defined as the extent of the shift in preference after the METH injection.

In vivo chemogenetic manipulation

For chemogenetics regulation of the mPFC-CL pathway, the rAAV2/9-EF1α-DIO-hM4D(Gi)-WPREs-hGH pA (PT-0987, 5E + 12 vg/mL, BrainVTA, China) or the rAAV2/1-hSyn-CRE-EGFP-WPRE-hGH pA (PT-1168, 1.07E + 13 vg/mL, BrainVTA, China) was bilaterally injected into mPFC, while the rAAV2/Retro-hSyn-Cre-EGFP-WPRE-hGH pA (PT-1186, 5E + 12 vg/mL, BrainVTA, China) or rAAV2/9-VGAT1-DIO-hM3D(Gq)-mCherry-WPRE-hGH pA (PT-1725, 5.20E + 12 vg/mL, BrainVTA, China) was bilaterally injected into CL. For chemogenetics regulation of the CL-mPFC pathway, the rAAV2/9-EF1α-DIO-hM4D(Gi)-WPRE-hGH pA (PT-0987, 5E + 12 vg/mL, BrainVTA, China) or the rAAV2/1-hSyn-CRE-EGFP-WPRE-hGH pA (PT-1168, 1.07E + 13 vg/mL, BrainVTA, China) was bilaterally injected into CL, while the rAAV2/Retro-hSyn-Cre-EGFP-WPRE-hGH pA (PT-1186, 5E + 12 vg/mL, BrainVTA, China) or rAAV2/9-VGAT1-DIO-hM3D(Gq)-mCherry-WPRE-hGH pA (PT-1725, 5.20E + 12 vg/mL, BrainVTA, China) was bilaterally injected into mPFC. CNO (2 mg/kg, i.p., Selleck, USA) was administered 30 min prior to CPP-Training or CPP-Test to inhibit or activate the specific neurons. Saline (0.2 mL) was used as the control vehicle.

For chemogenetics regulation of mPFC terminals in the mPFC-CL pathway and CL terminals in the CL-mPFC pathway, the rAAV2/9-CaMKIIα-hM4D(Gi)-mCherry-WPREs-hGH pA (PT-0050, 5.46E + 12 vg/mL, BrainVTA, China) was bilaterally injected into mPFC or CL, and the

cannula (mPFC, cat. #62123, O.D. 0.3 mm; CL, cat. #62104, O.D. 0.2 mm, RWD, China) was placed 100 μm above the CL or mPFC. For all cannula mice, CNO (1 mM, 50 nL or 200 nL, Selleckchem, USA) was infused 5 min prior to CPP-Training or CPP-Test via infusion cannulas at a flow rate of 20 nL/min by a syringe pump (RWD, China). Saline (50 nL or 200 nL) was used as the control vehicle.

Data analysis

Statistical analysis was carried out using GraphPad Prism 8.0.2 software. All data were presented as the mean ± SEM. The data were analyzed by unpaired Student's t test, paired Student's t test, One-way ANOVA and Two-way ANOVA with Sidak's multiple comparisons test. All statistical significance was set as $p < 0.05$.

Reporting summary

Further information on research design is available in the Nature Portfolio Reporting Summary linked to this article.

Data availability

Source data are provided with this paper.

Code availability

The present study did not use any custom code, and all analyses were based on published code.

References

1. Stoneberg, D. M., Shukla, R. K. & Magness, M. B. Global methamphetamine trends: An evolving problem. *Int. Crim. Justice Rev.* **28**, 136–161 (2018).
2. Keleta, Y. B. & Martinez, J. L. Brain circuits of methamphetamine place reinforcement learning: The role of the hippocampus-VTA loop. *Brain Behav.* **2**, 128–141 (2012).
3. May, A. C., Aupperle, R. L. & Stewart, J. L. Dark times: The role of negative reinforcement in methamphetamine addiction. *Front Psychiatry* **11**, 114 (2020).
4. Zhao, J. et al. Different roles of Rac1 in the acquisition and extinction of methamphetamine-associated contextual memory in the nucleus accumbens. *Theranostics* **9**, 7051–7071 (2019).
5. Mayo, L. M. et al. Conditioned preference to a methamphetamine-associated contextual cue in humans. *Neuropsychopharmacology* **38**, 921–929 (2013).
6. McKendrick, G. & Graziane, N. M. Drug-induced conditioned place preference and its practical use in substance use disorder research. *Front. Behav. Neurosci.* **14**, 582147 (2020).
7. Huston, J. P., Silva, M. A.dS., Topic, B. & Müller, C. P. What's conditioned in conditioned place preference? *Trends Pharmacol. Sci.* **34**, 162–166 (2013).
8. Terem, A. et al. Claustral neurons projecting to frontal cortex restrict opioid consumption. *Curr. Biol.* **33**, 2761–2773.e2768 (2023).
9. Terem, A. et al. Claustral neurons projecting to frontal cortex mediate contextual association of reward. *Curr. Biol.* **30**, 3522–3532.e3526 (2020).
10. Jobson, D. D., Hase, Y., Clarkson, A. N. & Kalaria, R. N. The role of the medial prefrontal cortex in cognition, ageing and dementia. *Brain Commun.* **3**, fcab125 (2021).
11. Taniguchi, H. et al. A resource of Cre driver lines for genetic targeting of GABAergic neurons in cerebral cortex. *Neuron* **71**, 995–1013 (2011).
12. Markram, H. et al. Interneurons of the neocortical inhibitory system. *Nat. Rev. Neurosci.* **5**, 793–807 (2004).
13. Isaacson, J. S. & Scanziani, M. How inhibition shapes cortical activity. *Neuron* **72**, 231–243 (2011).
14. Hu, Y. B. et al. Distinct roles of excitatory and inhibitory neurons in the medial prefrontal cortex in the expression and reconsolidation of methamphetamine-associated memory in male mice. *Neuropsychopharmacology* **49**, 1827–1838 (2024).
15. Smith, J. B., Lee, A. K. & Jackson, J. The claustrum. *Curr. Biol.* **30**, R1401–r1406 (2020).
16. Crick, F. C. & Koch, C. What is the function of the claustrum? *Philos. Trans. R. Soc. Lond. B Biol. Sci.* **360**, 1271–1279 (2005).
17. Madden, M. B. et al. A role for the claustrum in cognitive control. *Trends Cogn. Sci.* **26**, 1133–1152 (2022).
18. Takahashi, M. et al. Preferential arborization of dendrites and axons of parvalbumin- and somatostatin-positive GABAergic neurons within subregions of the mouse claustrum. *Neurosci. Res.* **190**, 92–106 (2023).
19. Graf, M., Wong, K. L. L. & Augustine, G. J. Neuroscience: a role for the claustrum in drug reward. *Curr. Biol.* **30**, R1038–r1040 (2020).
20. Zhao, Z. et al. Fine-regional role of the claustrum in anxiety and higher sensitivity to cocaine in adolescent cocaine-exposed male mice during adulthood. *J. Neurosci.* **44**, e0884232023 (2024).
21. Wang, Q. et al. Regional and cell-type-specific afferent and efferent projections of the mouse claustrum. *Cell Rep.* **42**, 112118 (2023).
22. Jackson, J., Karnani, M. M., Zemelman, B. V., Burdakov, D. & Lee, A. K. Inhibitory control of prefrontal cortex by the claustrum. *Neuron* **99**, 1029–1039.e1024 (2018).
23. Wang, Y. J. et al. The claustrum-prelimbic cortex circuit through dynorphin/κ-opioid receptor signaling underlies depression-like behaviors associated with social stress etiology. *Nat. Commun.* **14**, 7903 (2023).
24. Habib, R., Nyberg, L. & Tulving, E. Hemispheric asymmetries of memory: the HERA model revisited. *Trends Cogn. Sci.* **7**, 241–245 (2003).
25. Ocklenburg, S. & Guo, Z. V. Cross-hemispheric communication: insights on lateralized brain functions. *Neuron* **112**, 1222–1234 (2024).
26. Zingg, B., Dong, H.-W., Tao, H. W. & Zhang, L. I. Input–output organization of the mouse claustrum. *J. Comp. Neurol.* **526**, 2428–2443 (2018).
27. Euston David, R., Gruber Aaron, J. & McNaughton Bruce, L. The role of medial prefrontal cortex in memory and decision making. *Neuron* **76**, 1057–1070 (2012).
28. Goldstein, R. Z. & Volkow, N. D. Dysfunction of the prefrontal cortex in addiction: neuroimaging findings and clinical implications. *Nat. Rev. Neurosci.* **12**, 652–669 (2011).
29. Chevée, M., Finkel, E. A., Kim, S. J., O'Connor, D. H. & Brown, S. P. Neural activity in the mouse claustrum in a cross-modal sensory selection task. *Neuron* **110**, 486–501.e487 (2022).
30. Barrett, F. S., Krimmel, S. R., Griffiths, R. R., Seminowicz, D. A. & Mathur, B. N. Psilocybin acutely alters the functional connectivity of the claustrum with brain networks that support perception, memory, and attention. *NeuroImage* **218**, 116980 (2020).
31. Brown, J. W., Taheri, A., Kenyon, R. V., Berger-Wolf, T. Y. & Llano, D. A. Signal propagation via open-loop intrathalamic architectures: a computational model. *eNeuro* **7**, ENEURO.0441-19.2020 (2020).
32. Kaur, N. et al. Specification of claustro-amygdalar and palaeocortical neurons and circuits. *Nature* **638**, 469–478 (2025).
33. Rubinov, M. Circular and unified analysis in network neuroscience. *eLife* **12**, e79559 (2023).
34. Chao, O. Y., de Souza Silva, M. A., Yang, Y. M. & Huston, J. P. The medial prefrontal cortex - hippocampus circuit that integrates information of object, place and time to construct episodic memory in rodents: behavioral, anatomical and neurochemical properties. *Neurosci. Biobehav. Rev.* **113**, 373–407 (2020).
35. Sridhar, S., Khamaj, A. & Asthana, M. K. Cognitive neuroscience perspective on memory: overview and summary. *Front. Hum. Neurosci.* **17**, 1217093 (2023).
36. Smith, J. B. et al. A role for the claustrum in salience processing? *Front. Neuroanat.* **13**, 64 (2019).

37. Bae, J. et al. Claustral MeCP2 regulates methamphetamine-induced conditioned place preference in cynomolgus monkey. *Exp. Neurobiol.* **31**, 390–400 (2022).
38. Koga, K., Kobayashi, K., Tsuda, M., Pickering, A. E. & Furue, H. Anterior cingulate cross-hemispheric inhibition via the claustrum resolves painful sensory conflict. *Commun. Biol.* **7**, 330 (2024).
39. White, M. G. et al. Anterior cingulate cortex input to the claustrum is required for top-down action control. *Cell Rep.* **22**, 84–95 (2018).
40. Medina, C. et al. The role of the claustrum in the acquisition, consolidation and reconsolidation of memories in mice. *Sci. Rep.* **14**, 24409 (2024).
41. Zhou, T. et al. Mapping information flow between the inferotemporal and prefrontal cortices via neural oscillations in memory retrieval and maintenance. *Cell Rep.* **42**, 113169 (2023).
42. Husain, M. The human hippocampus contributes to short-term memory. *Brain J. Neurol.* **147**, 2593–2594 (2024).
43. Santori, A., Morena, M., Hill, M. N. & Campolongo, P. Hippocampal 2-arachidonoyl glycerol signaling regulates time-of-day- and stress-dependent effects on rat short-term memory. *Int. J. Mol. Sci.* **21**, 7316 (2020).
44. Ormond, J., Serka, S. A. & Johansen, J. P. Enhanced reactivation of remapping place cells during aversive learning. *J. Neurosci.* **43**, 2153–2167 (2023).
45. Nguyen, R., Sivakumaran, S., Lambe, E. K. & Kim, J. C. Ventral hippocampal cholecystokinin interneurons gate contextual reward memory. *iScience* **27**, 108824 (2024).
46. Euston, D. R., Gruber, A. J. & McNaughton, B. L. The role of medial prefrontal cortex in memory and decision making. *Neuron* **76**, 1057–1070 (2012).
47. Preston Alison, R. & Eichenbaum, H. Interplay of hippocampus and prefrontal cortex in memory. *Curr. Biol.* **23**, R764–R773 (2013).
48. Kim, J., Matney, C. J., Roth, R. H. & Brown, S. P. Synaptic organization of the neuronal circuits of the claustrum. *J. Neurosci.* **36**, 773–784 (2016).
49. Jackson, J., Smith, J. B. & Lee, A. K. The anatomy and physiology of claustrum-cortex interactions. *Annu. Rev. Neurosci.* **43**, 231–247 (2020).
50. Atlan, G. et al. The claustrum supports resilience to distraction. *Curr. Biol.* **28**, 2752–2762.e2757 (2018).
51. Liu, J. et al. The claustrum-prefrontal cortex pathway regulates impulsive-like behavior. *J. Neurosci.* **39**, 10071–10080 (2019).
52. Miller, D. R., Bu, M., Gopinath, A., Martinez, L. R. & Khoshbouei, H. Methamphetamine dysregulation of the central nervous system and peripheral immunity. *J. Pharmacol. Exp. Ther.* **379**, 372–385 (2021).
53. Shanley, M. R. et al. Estrous cycle mediates midbrain neuron excitability altering social behavior upon stress. *J. Neurosci.* **43**, 736–748 (2023).
54. Rocks, D., Cham, H. & Kundakovic, M. Why the estrous cycle matters for neuroscience. *Biol. Sex. Differ.* **13**, 62 (2022).
55. Hudson, A. & Stamp, J. A. Ovarian hormones and propensity to drug relapse: a review. *Neurosci. Biobehav Rev.* **35**, 427–436 (2011).
56. Bobzean, S. A., DeNobrega, A. K. & Perrotti, L. I. Sex differences in the neurobiology of drug addiction. *Exp. Neurol.* **259**, 64–74 (2014).
57. Pittenger, S. T. et al. Female rats display higher methamphetamine-primed reinstatement and c-Fos immunoreactivity than male rats. *Pharm. Biochem. Behav.* **201**, 173089 (2021).
58. Kvitsiani, D. et al. Distinct behavioural and network correlates of two interneuron types in prefrontal cortex. *Nature* **498**, 363–366 (2013).
59. Granger, A. J. et al. Cortical ChAT(+) neurons co-transmit acetylcholine and GABA in a target- and brain-region-specific manner. *Elife* **9**, e57749 (2020).
60. Kepecs, A. & Fishell, G. Interneuron cell types are fit to function. *Nature* **505**, 318–326 (2014).
61. Wang, Y. J. et al. The claustrum-prelimbic cortex circuit through dynorphin/kappa-opioid receptor signaling underlies depression-like behaviors associated with social stress etiology. *Nat. Commun.* **14**, 7903 (2023).

Acknowledgements

This work is supported by the National Natural Science Foundation of China (82271531 to X.G., 82405570 to Y.F.), Natural Science Foundation of Jiangsu Province of China (BK20240726 to Y.F.), and Traditional Chinese Medicine Technology Development Project of Jiangsu Province (ZD202302 to X.G., MS2022003 to Y.F.).

Author contributions

Y.H., Z.Z., and Y.L. performed the experiments and collected the data. Y.H., Z.Z., and Y.F. performed the data curation and analysis. Y.L. and Q.F. assist with data analysis and behavioral experiments. S.W. and W.W. assist with data analysis and behavioral experiments. Y.F., Y.H., and X.G. prepared figures and wrote the draft. H.Y.K. edited the manuscript. X.G. conceptualized the overall concept and supervised the project.

Competing interests

The authors declare no competing interests.

Additional information

Supplementary information The online version contains supplementary material available at https://doi.org/10.1038/s41467-025-68009-4.

Correspondence and requests for materials should be addressed to Yu Fan or Xiaowei Guan.

Peer review information *Nature Communications* thanks Junxu Li, Xiaojing Ye and Hu Zhao for their contribution to the peer review of this work. A peer review file is available.